DENSYS
MASTER ERASMUS MUNDUS | DECENTRALISED SMART ENERGY SYSTEMS

UNIVERSITÉ DE LORRAINE

POLITECNICO DI TORINO

Modelling of a SOFC-based micro-combined heat and power (m-CHP) system for a residential application

by

Sthefi Klaus

Academic Supervisors:
Massimo Santarelli
Marta Gandiglio

Industrial Supervisor:
Benoit Honel

A master thesis submitted in partial fulfilment
of the requirements for the degrees of

Master Energie parcours "Decentralised Smart Energy System"
in Université de Lorraine

and

MSc in Energy and Nuclear Engineering
in Politecnico di Torino

September 6th, 2023

You cannot get through a single day without having an impact on the world around you. What you do makes a difference, and you have to decide what kind of difference you want to make.

— Jane Goodall

Acknowledgements

The past 10 years of my life, since I decided to leave the comfort of my home to move to China, have been challenging, difficult, nerve wrecking, confuse, but at the same time amazing, filled of beautiful people and beautiful moments, full of learning and growing opportunities. When I took the decision of leaving Brazil, I was a kid, and I had not the slightest clue that my life would unfold this way, leading me here to this precise moment. I hold a deep gratitude to all the people my path crossed throughout the years. Each of you made an impact in my life, small or big, good or bad, I became a better person because of you.

So first and foremost, I want to start this section by thanking my mom, Carla Reichert, for pushing me to follow my dreams, even when that meant moving very far from her. For giving me the best education and teaching me from a young age that I was smart and capable, that I was not everybody, that I should always aim for the best, and if I worked hard enough, I could reach whatever I wanted. I would be nothing without you, and I love you more than anything.

I am also most thankful to Fabrice, the kindest person I've ever met. Fabrice, you are, unquestionably, the best coordinator a student can ask for, and even more, a friend. Your dedication to your job and family, and the way you manage to find a balance between this incredibly demanding position and the little pleasures of life is inspiring. I won't ever get tired of repeating, you are touching and changing the paths of each of our lives. DENSYS was easily one of the best experiences of my life, and I thank you for that.

But I can't mention my gratitude to DENSYS without mentioning Samira and Heathcliff. I am sorry we, DENSYS students, are quite a handful sometimes! It's always great to know we can count on you to help us solve all sorts of problems, organize everything, and assure the good functioning of the program. And you are the best company to go for a dinner or ice-cream and discuss the paradoxes of life and people in it. I also want to thank my academic supervisors Professors Massimo Santarelli and Marta Gandiglio, and Professor Olivier Herbinet, for extending their expertise and being available to answer my questions so I could reach good results.

I want to thank my colleagues and friends, Anjali and Jose, Piero, Kosta and Nikshan. You all helped me more times than I can count, you kept me company through the hard nights of study and innumerable projects, gave me advice, emotional support and followed my walking through the many new experiences I had to have. I will keep the moments we lived together in my memory and heart forever.

Next, I want to thank my Siemens supervisor, Benoit Honel, for guiding me through the work and always giving me great support and advice, while trusting my ability to take decisions on the work forward. I extend this thanks to Colas, thank you for helping me understand Amesim and debug my models more times than I can count! A special thanks as well to Alberto, the entire Elec team, and all of my colleagues in Siemens for receiving me and making me feel part of the team from the very first day, for patiently hearing my difficulties every morning in the daily and offering me support when things were not going well, or cheers when it suddenly worked.

But I could not finish a master's degree without a bachelors. So I also want thank my bachelor's professors, Isabel Malico and Eugênio Garção. You always believed in my capacity, and its thanks to you that I have the chance of being here today. Without your teachings, your support to keep the high goals throughout the course, and specially your incredible recommendation letters, I would never have this achievement. I also need to thank my colleague Lisa Bunge, for always keeping up the good competition and challenging me to perform better and better.

I also want to thank Kevin, for helping me in my internship and job search, but even more, for giving me the emotional support in all the moments where I started doubting myself. Thank you for keeping me well fed, and well cared for, and helping me take things a little bit less seriously. Thank you for helping me see and appreciate the simple moments in life.

Lastly, I think I deserve some gratitude for myself, for putting in a lot of hard work, for never giving up even when I really wanted to, for sacrificing social life, mental health and many hours of sleep to keep up with the delivery dates of projects. Thank you me for reaching this moment!

Executive Summary

A multi-physics process simulation software has become a fundamental instrument for managing the entire lifecycle of a product, from ideation to end-of-life. It accelerates the design and optimization of large systems, aiding in decision-making, engineering, and operation. With the recent growth of renewable energy systems and the push towards energy transition, it is necessary to develop new modules into the simulation tools to include new technologies.

Siemens is investing on that and is currently developing new modules for the inclusion of SOFC in their process simulation software Simcenter Amesim. In this context, the goal of this thesis is to develop and optimize a simulation model of a micro-combined heat and power (m-CHP) system based on the use of the Solid Oxide Fuel Cell (SOFC) for residential application.

To start, it was made a study of all the components that go into the inclusion of a SOFC into a residential house, their advantages, disadvantages, and limitations. Then, there was the study of the capacities of the Amesim libraries, development, and validation of the needed components such as the Fuel Cell, reformer and afterburner.

This was followed by the modelling in Amesim of a complete balance of plant of a SOFC fuelled by natural gas and applied into a residential house, with a sensitivity analysis to some of the most important inputs to the system. To finalise, it is presented a case study comparing the Fuel Cell system developed in terms of energy cost and carbon emissions to other ways of supplying the household demand, such as using only the electricity grid, a combination of power grid and natural gas or hydrogen.

The report is concluded with notes on the capacities and limitations of the model and suggestions to further improvements that can be implemented.

Table of Contents

Table of Figures

Table of Tables

1. About the company

This master thesis was written inside the R&D department of Siemens Digital Industries Software in Lyon, France, as part of the team working on the development of electrical and fuel cell tools for the software Simcenter Amesim. Siemens Digital Industries Software is a leading provider of software solutions and services for the digital transformation of industrial enterprises. The company's portfolio includes product lifecycle management (PLM) software, industrial automation, and software development tools, helping companies across various industries to improve their efficiency, optimize their digital workflows and drive innovation across industries.

2. Introduction

For many decades now, there has been an ever-growing discussion about climate change. It has become undeniable that actions need to be taken towards energy transition and more sustainable development. There is a slow shift of mentality all around the world, driven not only by environmental factors but also social, political, and economic considerations. As of December 2015, 196 countries/parties worldwide have signed the Paris agreement, pledging to limit the worlds temperature increase bellow 2°C above pre-industrial levels, with efforts towards a 1.5°C limit. [1]

According to the International Renewable Energy Agency (IRENA), the success on achieving a climate safe future depends on transforming the energy sector from fossil-fuels based to zero-carbon sources by the second half of this century. IRENA's roadmap position renewable energies (RE) and energy efficiency as the key drivers for CO_2 mitigation, followed by electrification, carbon capture and hydrogen technologies. [2] However, it is very clear for all that phasing out fossil-fuels is a very complex task, including innumerable challenges, such as technology development and deployment, infrastructure, policies and regulations, costs and investment, social acceptance, etc.

The worldwide investment on new renewable energy technologies, as well as the significant socio-political need for new climate change mitigation techniques, will need a paradigm shift away from regulated and centralized power generation and towards a decentralized system. The development of hydrogen solutions is taking the spotlight in recent times. In France, for example, it was put in place a National Hydrogen Strategy [3] for the 2020-2030 decade, with 7.2bn€ allocated to promote hydrogen into the French industry and mobility sector, promote H_2 electrolysis and storage technologies, develop up to 150 thousand jobs in the sector, among others. The aim is to make France a leading nation in green hydrogen production by 2030.

A considerable portion of the recent attention in hydrogen as a vector for energy transition has been focused on the use of Proton-Exchange Membrane Fuel Cell (PEMFC) to substitute internal combustion engines in automotive applications. This has somehow overshadowed the developments in the other types of fuel cell technologies, such as the Solid Oxide Fuel Cell (SOFC). The SOFC is currently not be the best fit for the integration with small vehicles, due to its high operating temperature (500°C – 850°C) and its slow start-up process, but it is very well in development and can be an excellent alternative to supply the energy needs in stationary applications. Its modular nature give it great potential for the end-use market sector. [4], [5]

It is important to choose the appropriate technology for each field of application. The SOFC technologies presents several advantages compared to other fuel cell (FC) technologies: It can be used in co-generation systems, providing not only power but also heating and cooling, and thus allowing an overall higher system efficiency; It uses in its construction non-precious catalysts; It can be adapted to be used in a reverse mode, to operate as an electrolyser and produce hydrogen; It is more resistant to sulfur contamination, and it can be used with multiple types of fuels, not requiring high purity hydrogen

like the PEMFC. [5] The fuel flexibility is one of the main advantages of the SOFC for residential and commercial applications, since it can smooth the transition between the carbon-based fuels, which are very well implemented in the current energy network, and a cleaner alternative in the future.

Fuel cell technologies are in stage of fast development. They have been extensively researched in terms of electrochemistry, materials, and stack construction, but there is a significant gap in the study of system integration and optimization. With this accelerated evolution, studies need to be conducted often to compare technologies and optimize the design process of such systems considering the most recent information available. There is currently limited research on the comparison of design, performance, and cost of FC technologies for small-scale stationary applications. The amount of system-level design research at lower than 10kW applications is insignificant compared to the larger scale (> 200kW) systems. While the technology is the same, the design constraints and hardware choices are fairly different for small and large-scale applications. [4]

Considering the urgency of all our climate goals, we currently take a very long time, even years, to get a project from ideation to design, regulations approval and construction. With the growth of all these new technologies, it is necessary to develop methodologies, models, and tools to facilitate and accelerate the design and optimization of such systems. There are still a lot of incertitude with new technologies, so having tools that correctly model the behaviour of a complex system can allow us to address system's design level issues. With multi-physics simulation tools, it is possible not only to compose and size a complex system much faster, but also to predict its use in multiple scenarios to find the most efficient design.

In this context, the primary objectives of this research are:

- To develop new tools into the process simulation software Simcenter Amesim for the inclusion of SOFC technology and its balance of plant (BoP).
- To validate and use these tools to develop a simulation model for a micro-CHP residential system based on SOFC.

As a broader objective, the model developed should be easily scalable and adaptable, making it an optimization tool for the design of SOFC/micro-CHP systems. It should allow to quickly predict the performance of the system, estimate the sizing requirements of the components and test the system response to different operating conditions and strategies. This model will then become a demonstrator that will be available for Amesim users as an example, to facilitate their own designs and parametrization of SOFC systems.

3. Literature review

3.1. SOFC principles and structure

The main principle of a Fuel Cell (FC) is to transform chemical energy into electrical energy via electrochemical reactions. It converts to electricity the energy released when a fuel breaks its chemical bonds to become a more stable molecule. The most traditional fuel is hydrogen gas, which is oxidized to water (H_2O) inside the FC. There are many types of fuel cells, and they are usually distinguished by the type of electrolyte used and the operating temperature. The most popular types are the alkaline FC (AFC), the polymer electrolyte membrane FC (PEMFC), the molten carbonate FC (MCFC) and the Solid Oxide FC (SOFC). This work will mainly focus on the SOFC.

The Solid Oxide Fuel Cell (SOFC) is a type of FC that is made of a solid-state ceramic material electrolyte, and operates in a range of temperatures between 500°C and 1000°C. It has the highest system

efficiency due to its potential for co-generation, and a high fuel flexibility compared to the other technologies.

The SOFC is composed of multiple cells that are assembled in series to compose a stack. Each cell is composed of two porous electrodes (called anode and cathode) separated by an ion-conducting electrolyte. A fuel (hydrogen, natural gas) is continuously supplied to the anode side and an oxidant (oxygen, air) to the cathode side. When a current is imposed, we force the reduction of oxygen at the cathode (R1). The ionized oxygen moves through the electrolyte membrane and reaches the anode, where it causes the oxidation of hydrogen (R1). The free electrons flow through an external electrical circuit to close the cycle.

(R1) Reduction @ cathode: $\frac{1}{2}\ O_2 + 2\ e^- \rightarrow\ O^{2-}$

(R2) Oxidation at anode: $H_2 + O^{2-} \rightarrow\ H_2O + 2\ e^-$

There are two base designs for the stack, planar or tubular. They present significant differences in terms of characteristics. Recently most effort is being put into planar cell/stack designs, which offer much higher volumetric power density and the potential for lower cost if the majority of the stack can be made of metallic rather than ceramic components.[6, p. 9] However, the planar design still presents some criticalities due to the seals and their behavior under thermal gradients.[7]

The working principle of the cell can be seen in Figure 1 and the structure of the stack in Figure 2.

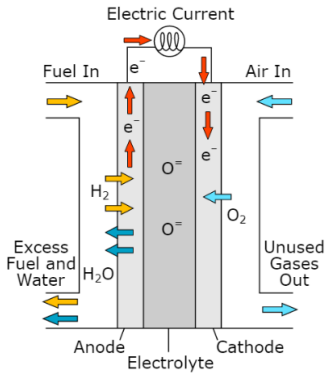

Figure 1: SOFC schematics [5]

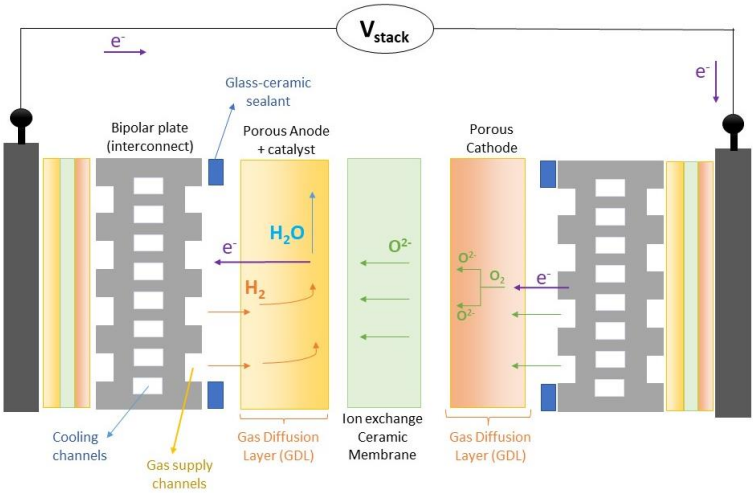

Figure 2: SOFC planar stack structure

There is constant research and development into the different materials for each of the FC components. Some of the trends in research aim at finding sulfur tolerant anode materials, lower

temperature operating electrolyte to enable the use of cheaper materials for all cell elements, higher thermal stress resistant materials, among others. [8] Some of the most well diffused materials used in SOFC can be cited as follows: [9]

- Bipolar plate: Can be metallic (usually ferritic chromium) or ceramic (such as doped lanthanum chromite perovskites).
- Electrolyte membrane: For temperatures above 700°C, we have Ytria-stabilized-Zirconia (YSZ), and CeO_2 for lower temperature, around 550°C.
- Anode : Nickel catalyzed YSZ (Ni-YSZ Cermet).

(LSM)

- Cathode: Strontium-substituted manganites such as $La_{0.8}Sr_{0.2}MnO_{3-\delta}$ (LSM), LSCF, $LaMnO_3$, $LaCoO_3$, etc.

3.2. Fuel Flexibility

It is well known that H_2 is the cleanest and most common fuel to be used directly in the fuel cell, having a high conversion efficiency and no CO_2 emissions. However, fuel flexibility is one of the main advantages of SOFC, since it can aid in the transition process between fossil fuels and cleaner energy sources. So it is important to look into different fuels that can be used in the SOFC and its different consequences.

If we use natural gas (mainly composed of methane) as a fuel, there are a series of reactions that can happen: Direct electro-oxidation of methane, methane cracking, methane steam reforming (MSR) associated with Water-gas shift (WGS), etc. As we can see bellow, multiple reactions can happen inside the reformer/fuel cell at the same time, but depending on temperature, pressure, chemical equilibrium, and catalytic conditions, some happen faster or more significantly than others.

Reforming reactions:

(R3) Methane Dry reforming: $CH_4 + CO_2 \leftrightarrow 2\ H_2 + 2\ CO$ ($\Delta H_{R,\ 298K}$ = +247 kJ/mol → endothermic)

(R4) Methane steam reforming: $CH_4 + H_2O \leftrightarrow 3\ H_2 + CO$ ($\Delta H_{R,\ 298K}$ = +206 kJ/mol → endothermic)

(R5) Methane steam reforming: $CH_4 + 2\ H_2O \leftrightarrow 4\ H_2 + CO_2$ ($\Delta H_{R,\ 298K}$ = +165 kJ/mol → endothermic)

Carbon deposition reactions:

(R6) Methane cracking: $CH_4 + \text{heat} \leftrightarrow 2\ H_2 + C$ ($\Delta H_{R,\ 298K}$ = +75 kJ/mol → endothermic)

(R7) Boudouard reaction: $2\ CO \rightarrow C + CO_2$ ($\Delta H_{R,\ 298K}$ = -172 kJ/mol → exothermic)

Water reactions:

(R8) Water gas formation: $C + H_2O \leftrightarrow H_2 + CO$ ($\Delta H_{R,\ 298K}$ = +131 kJ/mol → endothermic)

(R9) Water-gas shift (WGS): $CO + H_2O \leftrightarrow H2 + CO_2$ ($\Delta H_{R,\ 298K}$ = - 41 kJ/mol → exothermic)

Methane oxidation:

(R10) Methane Partial oxidation: $CH_4 + ½\ O_2 \leftrightarrow 2\ H_2 + CO$ ($\Delta H_{R,\ 298K}$ = -36 kJ/mol → exothermic)

(R11) Methane Full oxidation: $CH_4 + 2\ O_2 \leftrightarrow 2\ H_2O + CO_2$ ($\Delta H_{R,\ 298K}$ = -803 kJ/mol → exothermic)

Electrochemical reactions:

(R12) CO Oxidation: $CO + O^{2-} \leftrightarrow CO_2 + 2\ e^-$ ($\Delta H_{R,\ 298K}$ = -283 kJ/mol → exothermic)

(R13) Hydrogen Oxidation: $H_2 + O^{2-} \leftrightarrow H_2O + 2\ e^-$ ($\Delta H_{R,\ 298K}$ = -243 kJ/mol → exothermic)

The chemical equilibrium is the state in a reaction in which both the reactants and products are present in concentrations which have no further tendency to change with time. Equilibrium is attained

when the Gibbs free energy of the system is at its minimum value. As is shown in Figure 3, by calculating the point of chemical equilibrium for different thermodynamic conditions and with different mixtures of components, we can have an idea of what would happen inside the FC.

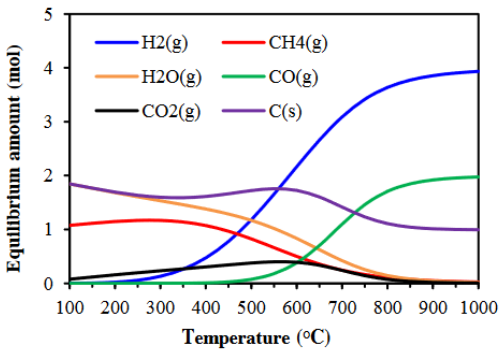

Fig. 3. Thermodynamic equilibrium of the mixture containing 2 moles of CH_4 and 1 mole of CO_2.

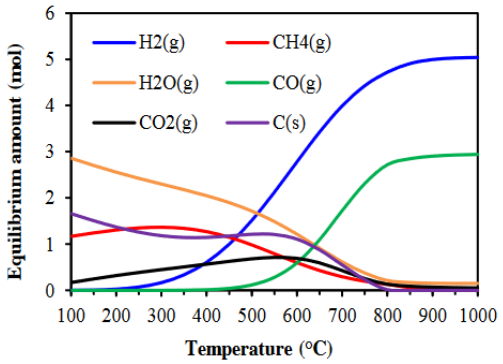

Fig. 6. Thermodynamic equilibrium of the mixture containing 2 moles of CH_4, 1.2 mole of H_2O and 1 mole of CO_2.

Figure 3: Thermodynamic equilibrium of methane dry reforming (on the left) and steam reforming (on the right) [10]

In general, reactions (R10) and (R11) – the direct oxidation of methane – are slower reactions, harder to achieve electrochemically and more likely to occur in a multi-step process.[11] Reaction (R6) – cracking of methane – is a reaction we want to avoid, due to the formation of carbon deposits on the surface of the anode, poisoning the catalyst and degrading the cell voltage.

Carbon formation and deposition is often controlled by kinetic phenomena (chemistry, mass transport, etc), but is only favored (driven by chemical equilibrium) when there is a low oxygen content in the mixture. The ternary diagram shown below can help to estimate, based on the C-H-O ratio of a mixture, the likelihood of carbon formation for different temperatures based on chemical equilibrium.

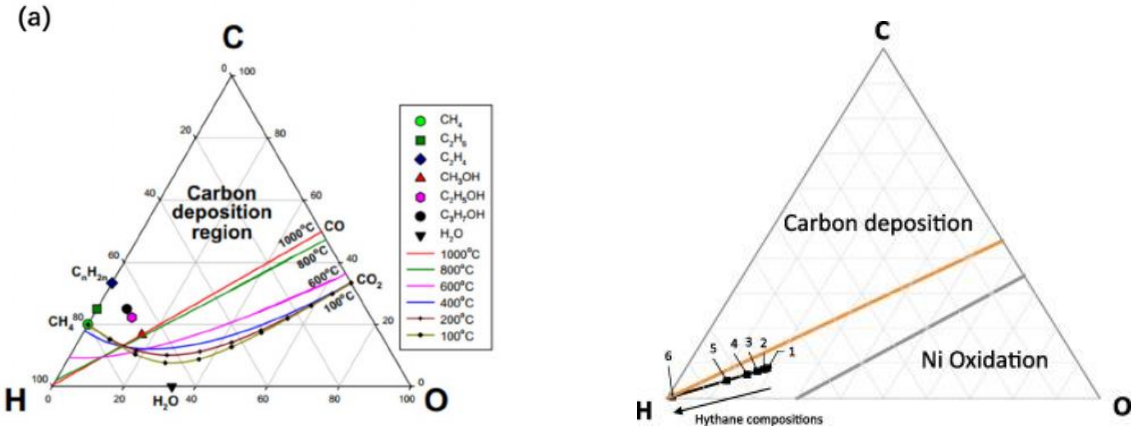

Figure 4: C-H-O ternary diagram at different operating temperatures [12], [13]

Because of this need for oxygen, the presence of steam in the fuel mixture is very important to push the intended reactions to happen. According to Minh et al., with temperatures above 800°C and H_2O addition to fuel during reforming, it is possible to avoid completely the carbon (coke) deposition and reach a very high methane conversion, as we can see in Figure 3. [10] Instead of providing steam externally to the anode inlet, it is also possible to have partial recirculation of the anode exhaust, which is rich in oxygen carriers like H_2O and CO_2 [14]

So finally, the MSR reaction will be the main objective for SOFC systems. For the methane reforming to happen, it's necessary temperatures between 700°C to 1000°C and pressure between 3 to 25 bar. [15]

Raising the temperature is one possible away to shift the equilibrium of reaction away from carbon formation zone.

It is also necessary to use a catalyst to favor the reaction. Nickel is one of the most used catalysts for this reaction, but its unfortunate that it is also a great catalyst for the methane cracking reaction. To solve carbon deposition problem, some researchers have tried changing anode materials, structure and catalyst, but this can proof limiting to the operating conditions and fuel flexibility.[16]

After the MSR reaction happens at the anode, as can be seen in Figure 5, it is followed by a water-gas shift, and the total hydrogen formed in these 2 previous reactions goes through oxidation to close the fuel cell cycle. The reduction reaction at the cathode continues the same as when using pure hydrogen, like in Figure 1. [10]

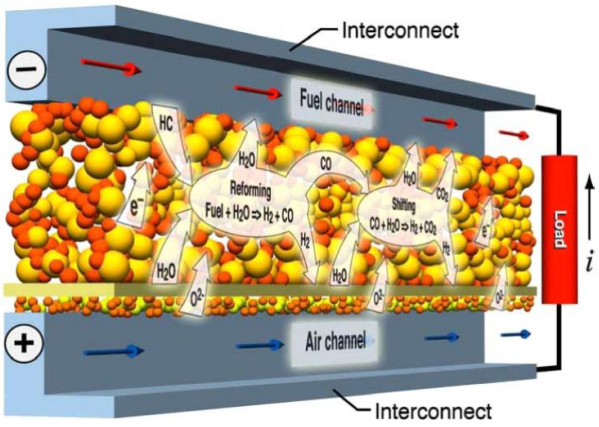

Figure 5: internal reforming of methane in SOFC [5]

There are quite a few problems that come with operating the SOFC with gaseous fuels such as hydrogen or methane. The main ones are linked with the low density of these fuels, meaning that to store and transport them it is required either huge volumes, very high compression or cryogenic cooling, all very energy consuming processes. One way of avoiding those issues is to use a fuel that is liquid in atmospheric conditions, which rises our interest in methanol. Besides its high volumetric energy density, methanol can be easily obtained from natural gas, agriculture's byproducts, municipal waste, etc, and because its composition already includes some oxygen, it is much less prone to carbon deposition.

Yanlei et al. found that in direct internal reforming of methanol (for a Ni-YSZ anode-supported SOFC operating at 750°C), using dry methanol lead to a very poor cell performance, having an unstable behaviour and durability of only 11 min; using a steam to carbon (S/C) ratio of 1 also lead to poisoning and degradation of the cell voltage after 36 hours. However, using a (S/C) ratio of 2, no carbon deposition was found. It was also found that the cell using methanol could reach about 90% of the power density of the one using H_2 directly.[16]

(R14) Methanol steam reforming: $CH_3OH + H_2O \rightarrow 3\ H_2 + CO_2$ ($\Delta H_{R,\,298K} = +49$ kJ/mol → endothermic)

(R15) Methanol decomposition: $CH_3OH \rightarrow 2\ H_2 + CO$ ($\Delta H_{R,\,298K} = +91$ kJ/mol → endothermic)

Several researches using ethanol or even gasoline as a fuel highlight the difficulties with avoiding carbon deposition. To use ethanol as a fuel, temperatures even higher than 1000°C could be required and with a steam-to-fuel ratio over 4.5, which imposes different constraints on the materials and structure of the SOFC. In general, investigation results indicate that feeding various fuels in the same system may present major thermal management issues. Proper operation on different fuels may require significant modifications in operating conditions or system design. [11], [14], [17]

There are also literature investigating the performance of ammonia fed SOFC for power generation, which found that NH_3 is a technically feasible fuel for direct use and can have performances comparable or even better than that of H_2 fed SOFC.[18]–[20]

(R16) Amonia cracking/decomposition: $2\ NH_3 \rightarrow 3\ H_2 + N_2$

($\Delta H_{R,\ 298K}$ = kJ/mol → endothermic)

(R17) Amonia oxidation: $2\ NH_3 + 5\ O^{2-} \rightarrow 2NO + 3\ H_2O + 10\ e^-$

($\Delta H_{R,\ 298K}$ = kJ/mol → endothermic)

(R18) Selective catalytic reduction (SCR) of NOx: $2\ NH_3 + 3\ NO \rightarrow {}^5\!/_2\ N_2 + 3\ H_2O$

($\Delta H_{R,\ 298K}$ = kJ/mol → endothermic)

About the topic on maintaining the humidity of the cell, PEMFC requires a very strict control of the humidity of the fuels and membrane to maintain ionic conductivity, which is not the case for SOFC. As we saw in the section on Fuel flexibility, SOFC requires, if operated with a carbon based fuel, the introduction of steam, and some control needs to be done between avoiding carbon deposition but not over-diluting the fuel. In PEM, however, the water plays a different role, and a very strict controlling is needed to maintain high humidity throughout the cell and avoiding condensation.

3.3. SOFC Balance of Plant

The Balance of Plant (BoP) layout that accompanies the SOFC depends on several factors, being the most significant the choice of fuel and application. Various BoP layouts are discussed in the literature, but they usually share five fundamental sections:

- Clean-up, gas purification and processing (in the case of use with fuel other than pure hydrogen)
- Fluid supply
- Electrochemical core
- Power conditioning
- Heat integration

We can see in Figure 6 a simple scheme for the BoP of a SOFC system fueled by natural gas. More detailing about each component of the system will be discussed in section 4.3 - Components description.

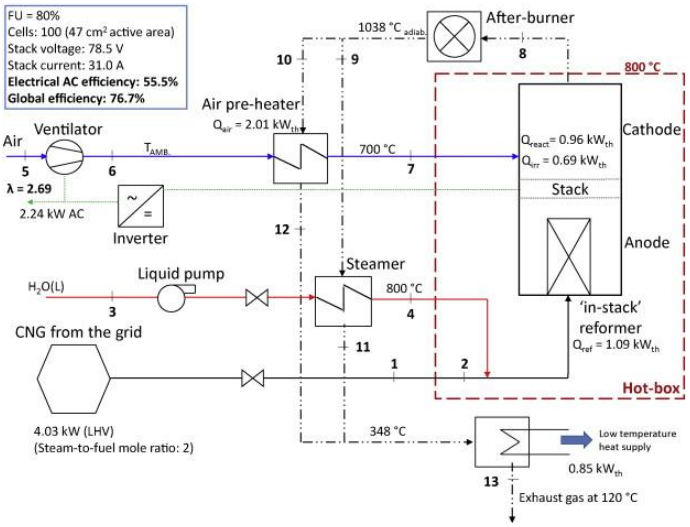

Figure 6: 2.24 kW SOFC+CHP for residential application [14]

3.4. SOFC in residential applications

Due to its high temperature of operation, SOFC can produce heat as a by-product of the electricity production. To increase efficiency and reduce the energy waste, SOFC is often coupled to several types of heat recovery units. Such combined generation systems can have expected efficiencies over 90%. There are many different possible architectures for this integration, and the design of the system is very dependent on the local conditions and end use of the energy. [5], [18] The SOFC can be associated to systems from W to MW scale, it can be integrated to co/tri/polygeneration systems, combined cycle power plants, renewable energies, etc. In summary, it can be suitable for all sorts of stationary applications. There are also investigations on how to adapt the SOFC technology to portable and mobility applications, such as trucks, trains and ships, but there are several cell, stack and energy management problems that need to be addressed to further this developments. [18], [21]

SOFC is often thought for large scale or industrial applications, due to its range of temperature for operation, but recently there are more and more initiatives to integrate it to residential or commercial buildings, due to its capacity to provide electricity, heat and even cooling and because it can operate with carbon-based fuels, differently from the PEM fuel cell. According to Ramadhani et al. [22], there is recently an increased interest SOFC-based polygeneration systems for residential, which was triggered by the prediction of the price reduction of SOFCs for the next five to ten years. He points out, as shown in Figure 7, that there is a growing trend in the number of publications about this type of systems.

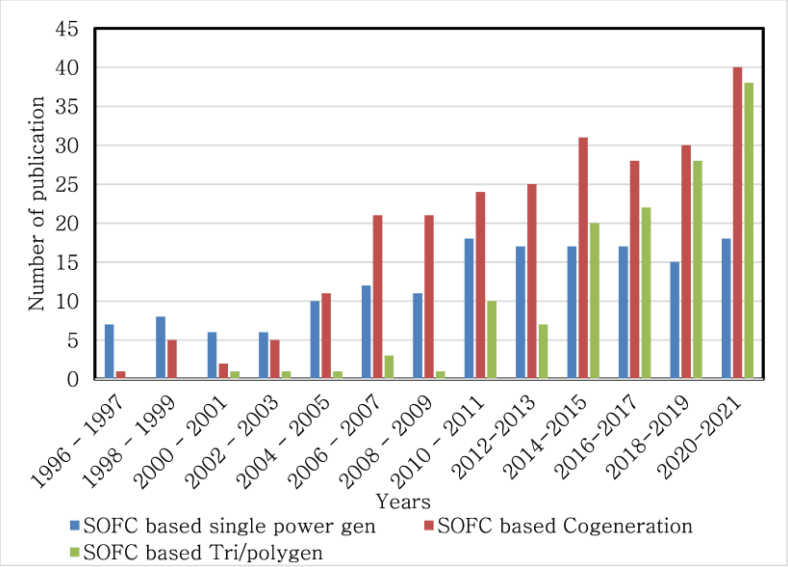

Figure 7: Trend of publication numbers for SOFC power generation in residential applications.

One very well developed study on the application of SOFC with focus on residential applications dates back to 2002. Dr. Robert J. Braun, in his PhD thesis, attempted to use modeling and simulation to develop an optimal design and operational strategy with focus on residential application in 2002. He finds the optimal cell design voltage, fuel utilization, and operating temperature parameters by the minimization of the life cycle costs. He concluded that hydrogen-fueled SOFC systems demonstrate lower system efficiencies than methane-fueled systems due to their higher air-blower power requirement and higher energy input for a same current output. He also studied different operating strategies (base-load or load-following and cogeneration or electric-only), finding that, when the system is sized correctly, base-load operation is economically more favorable than load-following for the grid-connected application. He already found back then efficiencies of 45% electric (LHV basis) and 85%

cogenerative, and simple payback time of 5-8 years for 1-2 kW SOFC systems in a high volume manufacturing market (mature cost). [4]

Dr. Braun further confirmed his findings in publications in 2006 [23] and 2010 [24]. In the latest, he further described that CHP systems achieved lower life-cycle costs of 9% to 23% when compared to their electric-only counterpart. Electric-only systems typically favored higher cell voltage and higher fuel utilization design points (around 85%), while m-CHP systems prefer a lower fuel utilization (around 75%), compensating the reduced electric efficiency by the waste heat recovered and the reduced parasitic consumption from higher fuel cell efficiency and lower electrochemical heat release. However, reducing fuel utilization beneath 75% is constrained by satisfying minimum system stoichiometric airflow requirements. He also concluded that SOFC-CHP systems can be applied to multifamily residential settings to benefit of the economy of scale.

Tan et al. highlight in their review of over 40 design studies from 2005 to 2019 on SOFC-based energy systems for buildings that even if the SOFC can operate with a very wide range of fuel compositions, currently natural gas is the only choice of fuel for SOFC in buildings, due to its lower cost, readily availability and already existing city infrastructure. They suggest that the association of the SOFC with other renewable energies or exchanging the fuel to biogas might be a good way to address the environmental concerns related to CO_2 emmisions. [25]

There are several studies analyzing the feasibility of SOFC cogeneration systems and demonstrating an appropriate performance to provide for the power and hot water demands of a single-family household, both in standalone and grid-connected modes, and even including the integration with an EV charging station. [26] [27] [28] It is also estimated that that the BoP of the SOFC-based m-CHP system is the most sensitive part of operation, accounting for 55% of system failures. [29]

Figure 8 shows some possible architectures for the integration of SOFC to a m-CHP system.

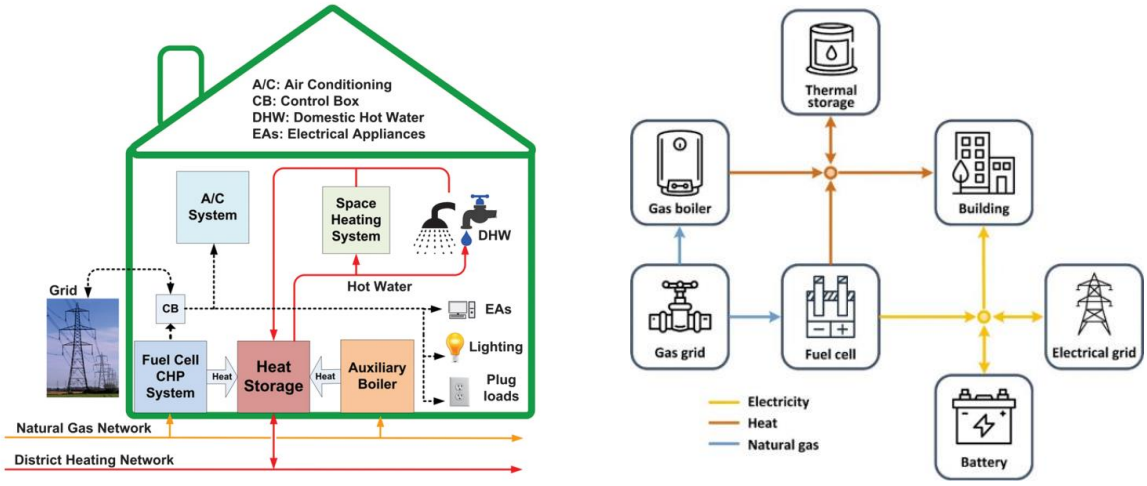

Figure 8: Integration of a SOFC-CHP system into a residential building [30], [31]

In 2016, Akikur et al. found that for a residential system including solar PV, reversible SOFC and hydrogen storage, for a single family in Malaysia and using 2016 prices, the payback time of the system could be 31 years. They expect it to lower to 21 years by 2020. They also highlight the importance of scale, since even with prices of 2016 it was possible to reach a 19 years payback time if the system was projected for 100 families instead of a single household. [32]

By 2023, fuel cell cogeneration systems can already reach 90 % efficiency, being 60 % electric and the remainder as thermal. But despite their great efficiency and potential, m-CHP systems are not yet at their full commercial stage.

The EU funded project HEATSTACK, under the Horizon 2020 program, tried to reduce the systems costs by reducing production costs of the two most expensive components of the fuel cell system: the fuel cell stack and heat exchanger. This was done by 2 approaches: development of tooling and processes to improve the manufacturing processes, increasing quality and reducing manufacturing time, and improvement of the durability such that the m-CHP system as a whole has a longer life. [33]

As shown in Figure 9, the ceramic cell costs could be drastically reduced with a larger production scale, from 8482.51 USD/kW to 1183.04 USD/kW (for a 1kW system), when the annual production increases up to 50,000 units per year. Talking about the full system cost, the BOP is the most representative part, representing 44.6 to 56.5% of total cost for small size systems. [29]

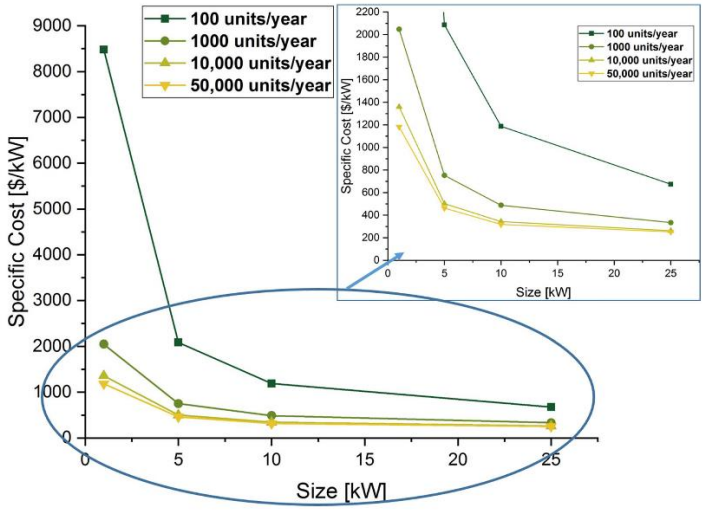

Figure 9: SOFC Ceramic Cell Potential Cost Breakdown [29]

Accordingly to extensive research from Cigolotti et al. [29], Europe and Japan are leading the market of residential m-CHP systems. This is mainly thanks to subsidies and programs and having several manufactures involved in the market.

Table 1: Some manufacturers involved in the market (adapted from [29])

Country/State	Manufacturer	Electrical Output [kW]	Electric Efficiency [%]	Total Efficiency [%]
Europe	Bosch	1.5	60	Up to 88
	SOLID Power	1.5	Up to 57	Up to 90
	Sunfire	0.75	38	88
Japan	AISIN	0.7	55	87
	Kyocera	0.4	47	80
	Osaka Gas [34]	0.7	53.5	87

Japan is the main leader in FC-based m-CHP unit installations, with the ENEFARM program. They reached a price of USD 8800/unit for SOFC and installed over 360 thousand units by 2020 (62% PEMFC and 38% SOFC). [29] Europe has installed more than 4100 fuel cell (both SOFC and PEMFC) units for m-CHP applications thanks to many demonstration projects. The three main projects responsible for this are Callux [35] claims 474 units installed between 2008 and 2015, Ene.field [36] reached 1046 installations between 2012 and 2017, and PACE is developing over 2500 systems between 2018 and 2023. [37]

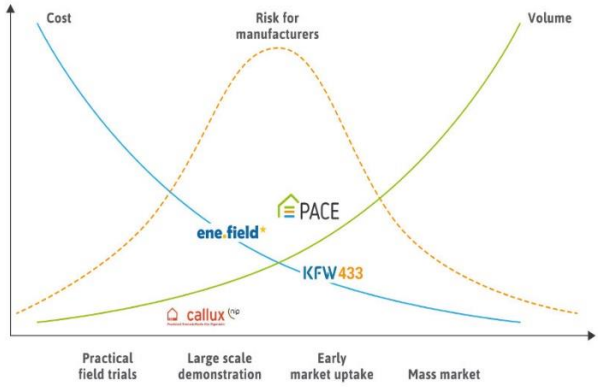

Figure 10: European Fuel Cell demonstration projects

In summary, in terms of technical feasibility, the SOFC is a great asset to be integrated to m-CHP residential systems. However, the economic assessment still poses limitations worldwide. The main disadvantage of this kind of systems is its very high initial investment cost. It will be necessary the economy of scale and increased incentives, allowing a significant price reduction, to reach economically attractive energy systems.

3.5. SOFC Start-up procedure

Due to the high operating temperature (700 – 1000 °C), the SOFC has to undergo the heat-up and start-up processes to reach operable conditions. This is a very relevant point, since it can pose limitations when deciding on the operating strategies of the SOFC and planning of the energy management system.

The heat-up process is to warm-up the cell from the room temperature (25 °C) to the operable level (around 600-800 °C). If the cell temperature rises too fast, it will lead to a serious internal temperature-gradient increase and significant differences of the thermal-expansion rates of the cell components, resulting in a high thermal stress and reducing the cell performance and its durability.[38] In the heating phase the system's temperature is increased by auxiliary heaters by heating a safety gas and passing it through the cathode and anode;

During the heat-up procedure, the temperature is being elevated and some reduced oxygen can flow from the cathode to anode through the membrane and end up oxidizing the nickel cermet anode. To avoid the oxidation of the nickel in the anode substrate, the flow gas has to remain at reduced state to ensure that no reduced oxygen is transported to anode. The first signs of the oxidation of the nickel catalyst occur as low as 290 °C and it proceeds more and more rapidly as the temperature increases. [39]

Therefore, it is necessary to feed reducing gas to the stack during the heat-up cycle to displace the oxygen in the fuel system and to protect the stack. This flow needs to be sustained for several hours during the system heat-up and cool-down, while the stack temperature is still high enough for significant re-oxidation. The most straightforward way to provide a reducing gas supply is to utilize gas containers of a premixed safety gas, which is often composed of pure nitrogen or a hydrogen-nitrogen mixture. There are also studies on how to heat-up a SOFC without a safety gas, possibly using multi-stages heating and pre-reforming. [39]

During this phase no electrical power is extracted from the system. In Figure 11, we can see the dynamic of temperature during the heat-up (and start-up) of a SOFC in which heat transfer gas is used to increase the temperature at a rate of 1.308 K/min for air and 1.56 K/min for fuel, respectively. [40]

For an optimal heat-up process, the required time should be minimized while the temperature gradient should be maintained under an allowable threshold. Chen et al. found that the counter-flow configuration is superior to the others as far as the heat-up time and the required energy are concerned, although it yields a relatively higher maximum-temperature-gradient. [38]

During the start-up procedure, also called power-ramping, the chemical compositions of the two feed gas streams are changed (anode hydrogen up and nitrogen down, cathode oxygen up and nitrogen down), along with power ramp-up (531 W/min in the example in Figure 11) until the target design point has been reached. The temperature of the solid eventually exceeds that of the fluids due to the electrochemical reactions. Once power ramping is initiated, the FU changes rapidly until it reaches its steady state conditions. The most important factor affecting the start-up time is the response of the stack temperature. To accelerate the start-up process we can increase the inlet pressure. [40], [41]

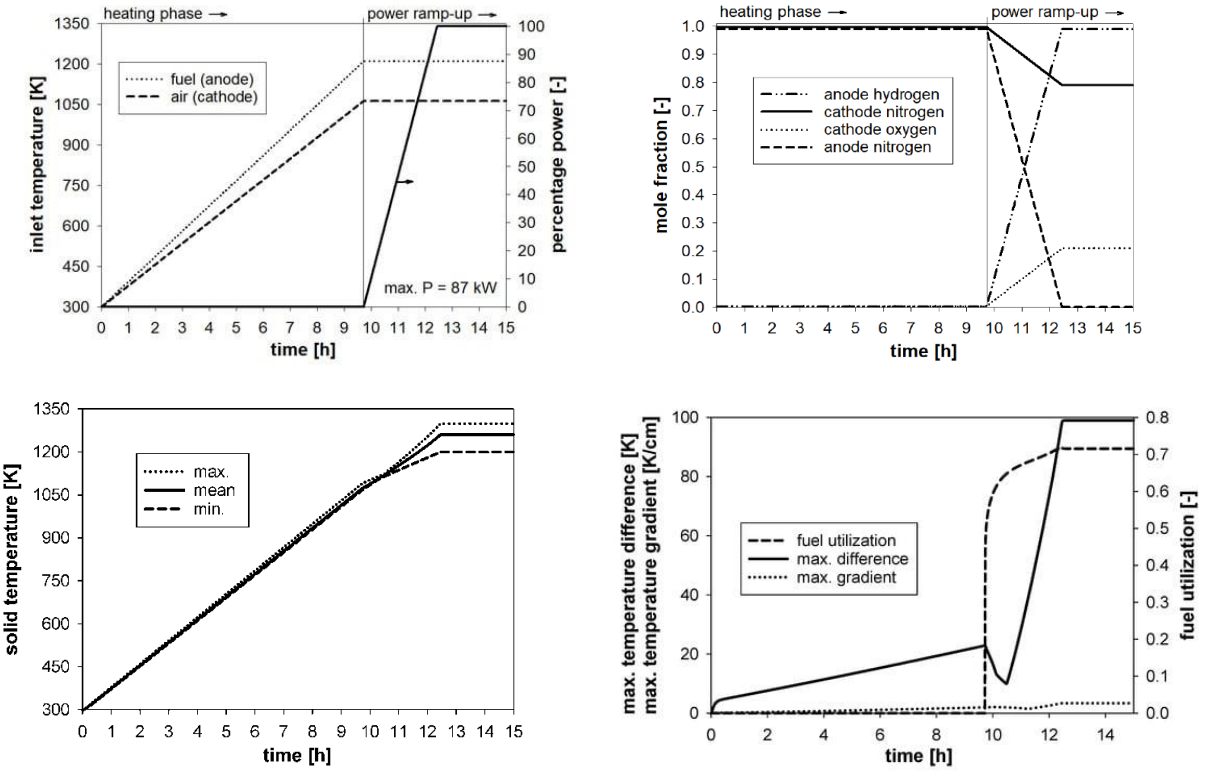

Figure 11: Heat-up and start-up processes of SOFC [40]

In terms of time, heat-up and start-up times depends very much on the geometry and materials of a particular FC. It's also dependent on the operating strategy used, limit of fluids velocity and temperature gradients inside the FC, the threshold for thermal stress, etc. There is literature for heat-up times from 5 minutes up to more than 15 hours. [42] A way of avoiding this extremely high start-up time could be to operate at partial load during the low demand periods of the day, resulting in significant losses associated with low conversion efficiencies and potential over-generation.

3.6. Operating Strategy

When we integrate a fuel cell to an energy system, there is a multitude of factors to balance. While the main objective is to meet all the energy demand, the energy flow and the role of each energy generator or sink can be optimized in many different ways depending on the application. The most

conventional approach is to control the energy generation based on the electrical and/or thermal loads. This approach usually can consist of different techniques, such as: base-load, following thermal load (FTL), following electrical load (FEL) and combined FEL and FTL strategies. [43]

- **Base-load or fixed-load:** the fuel cell operates at constant power, and there are auxiliary energy storage and generation methods to handle the balance of the load. When the power of the FC is higher than the load, energy is stored or sold to the grid, and when the load is higher, there is the use of the stored energy or grid to meet the needs.
- **FEL:** the fuel cell is run based on the electrical load profile, with its power output variating to meet the electrical demand and without considering the thermal load. The heat needs are only partially meet by the FC with the remaining heat coming from an auxiliary heating system.
- **FTL:** operates the FC with the goal of meeting thermal demand. If the electrical load cannot be met, it can use import from the electrical grid to reach the needs. A heat storage system can be included to improve system's efficiency.
- **Combined FEL and FTL:** When the electrical or thermal source produces more energy than can be used, there is energy and efficiency loss. To avoid that, its possible to use a hybrid approach with the FEL and FTL. There are many techniques to achieve that, such as seasonal operation strategy, time-based, emission-based strategy and economic-based and energy-storage-based strategy.[43]

In summary, when choosing an operating strategy for the system, the fuel cell is not going to be capable to meet perfectly electrical and thermal needs at all times. In any method of operation chosen, electricity and/or heat may be available when it is not needed or vice-versa, so there is always the need for a supporting storage/generation system. Furthermore, the efficiency of the FC and overall energy system is going to depend on the voltage-current characteristic and how far from the nominal power the stack is operated. According to Braun [4], the system design will depend on: (i) selection of optimal fuel cell design and operating point, (ii) heat recovery design, (iii) electric and thermal load management, and (iv) the performance characteristics of auxiliary hardware, such as inverters, pumps, compressors, controls, and external reformers (if any).

There are advantaged and disadvantages to each method of operation. With the SOFC, its important to note still that the start-up time, as discussed before, is quite slow and the stack is very subject to thermal stresses, so ideally it has to avoid thermal cycling by staying ON most of the time or staying in hot stand-by (where the temperature is kept constant even if the equipment is not operating). Besides that, when used in load-following, there is a time lag in the demand response depending on the electrochemical, thermal and mechanical characteristics of the stack and also the ability of the auxiliary systems such as temperature control and fuel supply to react quickly.

To give an example on the time response of SOFC, according to Zhang et al. [44], in SOFC integrated to gas turbines, demonstrations of rapid system response involving real hardware have been limited to modest load changes (<20%) over multiple hours. In the same paper they develop a system to operate around 50% ramp-down in 10s, but further studies are needed to overcome the difficulties presented in the study. Overall, the design of the stack and control system for load-following can be significantly more complex and implicate a significant price increase.

In 2002, Braun [4] found that for smaller sized systems, the base-load operation is economically more favorable than load-following for a grid-connected application. However, there is growing number of publications in more recent years studying different strategies for load-following in SOFC. For this

study, I could not find a recent in-depth comparison of different operating strategies taking into account newly developed strategies.

3.7. Fuel Cell Modelling

The modelling of a fuel cell system can be done in many different ways, depending mainly on what is the final use of the model. As described by Nagel [5], the most common approaches are as follows:

- Molecular level (nm-scale): Deals mainly with the reaction kinetics and are usually used to find the rate limiting reaction steps.
- Electrode level (μm-scale): These models deal with what is happening at anode or cathode level, and typically output the voltage losses for a given current density, temperature and set of geometrical and structural details of the modeled SOFC.
- Cell level (mm-scale): Also referred to as repeat element models, they output voltage, mass and energy balances, allowing prediction of local cell operating conditions. Commonly used to investigate cell design parameters such as cell length, channel width and flow path.
- Stack level (cm-scale): Are usually three-dimensional models with the stack discretized in many elements, allowing the mass and energy balances to be solved for every point of the system. They are used to investigate the impact of realistic boundary conditions in a stack, such as the impact of different cell and stack geometries and their impact on the temperature and current density distribution.
- Plant level (m-scale): These models analyze the interaction between the FC stack and the balance of plant components (pumps, compressors, heat exchangers, etc). It is generally used to optimize the plant design and improve system's efficiency.

The use of lumped models is the most commonly used approach, where an extrapolation of electrode level model results are used for the plant level systems analysis. The lumped model generally has as assumptions that all chemical and electrochemical reactions involved reach equilibrium and it uses Faraday's Law and stoichiometry to determine the fuel and oxygen input requirements. The fuel utilization and current density are inputs to the model and the power is an output. The voltage can be a given fixed value, can be determined by a given polarization curve (U-I curve) or calculated by the correlations involving the Nernst voltage and voltage losses mechanisms. One of the main problems with this type of lumped model is that in reality the gas composition and the temperatures change along the fuel channel, which is hard to capture without a discretized model. [5]

4. m-CHP system modelling

4.1. Methodology

For this thesis, the modelling of the system will be done with a lumped approach. Each component of the system is modelled as an individual component using the multi-physics method in the software Simcenter Amesim. Each component is connected to the system as a black-box, and inside each it is applied the necessary physical and chemical relations to simulate accurately the behaviour of this component in the system given the inputs and estimate the output. All systems respect the energy and mass balances, as well as the necessary relations specific to each component.

The methodology for this study was the following:

- Study of the micro-CHP systems integrating SOFC.
- Decision on the system components and design objectives
- Study of the modelling approach of components already implemented in Amesim
- Modelling and implementation of the components not previously included in Amesim
- Validation of the performance of the newly designed components
- Research of parameters needed as input to the system components
- System integration in Amesim
- Evaluation of system's results

In practice, some of these steps were done in parallel instead of sequentially.

4.2. Guidelines for the system design

There are an infinite number of possible solutions for the design of an energy system. An optimal demand response has to take in consideration a very large set of constraints and it is often studied case-by-case. After a preliminary study of combined heat and power systems, the factors present in Figure 12 were highlighted as main design decisions criteria. In the colorful blocks are the main topic and listed below are some of the main options available in reference.

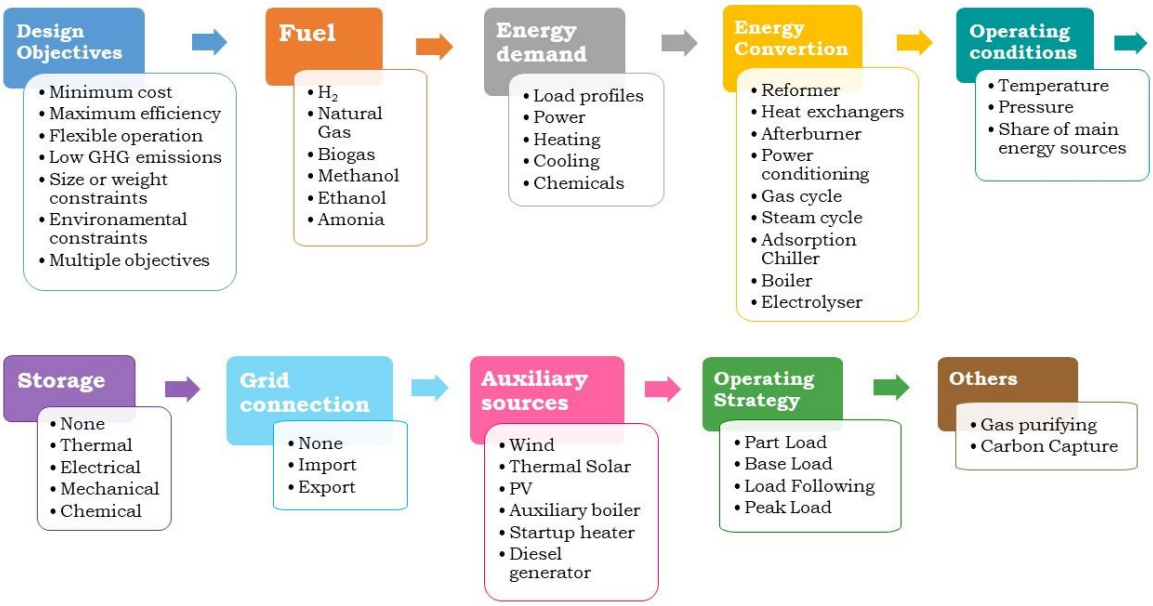

Figure 12: Design decisions for CHP system

In the next sections I will detail each of the system components, describe the decisions taken in reference of each one and their modelling approaches.

4.3. Components description

4.3.1. Gas clean-up

To proceed with the design, it is necessary to choose the type of fuel that is going to be used. According to Braun et al. [23], when considering residential applications, hydrogen-based SOFC

systems do not offer better performance compared to methane-based SOFC systems. He actually found up to 6% better efficiency in the methane-fuelled system.

Considering that this system is thought for a residential application, where usually there is already some kind of infrastructure in place for the supply of natural gas, this is going to be the chosen fuel for the initial design. Furthermore, the design of systems that can be compatible with current infrastructure and easily changed to a cleaner fuel in the future is a step forward in facilitating the transition and diffusing application. Later on, this system model can be adapted and even used for the comparison of performance with different fuels.

The composition of natural gas depends on the conditions and place where it was formed. It can contain anywhere between 81 and 97% of methane. An example of composition of NG is presented in Table 2: Example of Natural Gas composition in EuropeTable 2. [45]

Table 2: Example of Natural Gas composition in Europe

Component	Composition
Methane (CH_4)	90%
Ethane (C_2H_6)	5%
Propane (C_3H_8)	1%
Butane (C_4H_{10})	0.2%
Nitrogen (N_2)	2.2%
Carbon Dioxide (CO_2)	1.4%
Sulfur (H_2S)	< 10 mg/m³

For this study, we are using as the composition of NG the following fractions: 96.2% of CH_4, 1.4% of CO_2 and 2.2% of N_2. There is no inclusion of ethane, propane and butane due to the limitations of the reformer model, which are explained in section 4.3.3.

The natural gas often can contain some contaminants such as sulfur, which can be highly reactive with the Nickel in the fuel cell catalyst, quickly deactivating it and poisoning the FC. The SOFC can usually withstand between 1-10ppm of sulfur, so depending on the composition of the fuel obtained, a desulfurization treatment needs to be applied. [4] The fuel pre-processing is not included in this model and should be addressed in future work.

4.3.2. SOFC

The functioning of a fuel cell is determined by the thermodynamics of the reaction. Knowing the Gibbs free energy and enthalpy of a reaction helps to determine the spontaneity of the reaction and which temperatures favor the direction of reaction. Exothermic reactions will function better at lower temperatures, while endothermic reactions are favored by high temperatures. However, only thermodynamics are not enough to predict the behavior of the cell. We need to determine the kinetic factors, which will tell how fast a reaction will reach its equilibrium based on the movements of the atoms. In general, the higher the temperature, the better the atoms mobility, thus faster reactions.

The SOFC model implemented in Amesim follows the scheme presented in Figure 13. The gas channel and the electrodes are represented as gas volumes and the diffusion of the components between them is dealt with by a component that models the gas diffusion and thermal conduction through porous media. The electrochemical reactions happen inside the volume that borders the membrane, and the rate

of the reactions, energy and mass balances, as well as the polarization curves are handled by the SOFC component, which represents the membrane and current collectors.

The fuel utilized in the fuel cell is mainly composed of methane, which, as seen in the reactions presented in section 3.2 - Fuel Flexibility, is going to be reformed and convert mostly into CO and H_2. Simultaneous oxidation of the H_2 and CO then takes place in the FC. According to a study made by Andreassi et al. [46], the CO oxidation provides a contribution of 12.5% on the current basis, meaning that ignoring the CO and using only H_2 as the reductor can cause an underestimation of the voltage, specially at high current densities.

Considering this, the cell voltage is calculated according to the equivalent parallel electrical circuit analogy described by Andreassi et al. [46] and the commonly accepted equations for the voltage irreversibilities, which are explained in more details in [47]. The circuit used is presented in Figure 14.

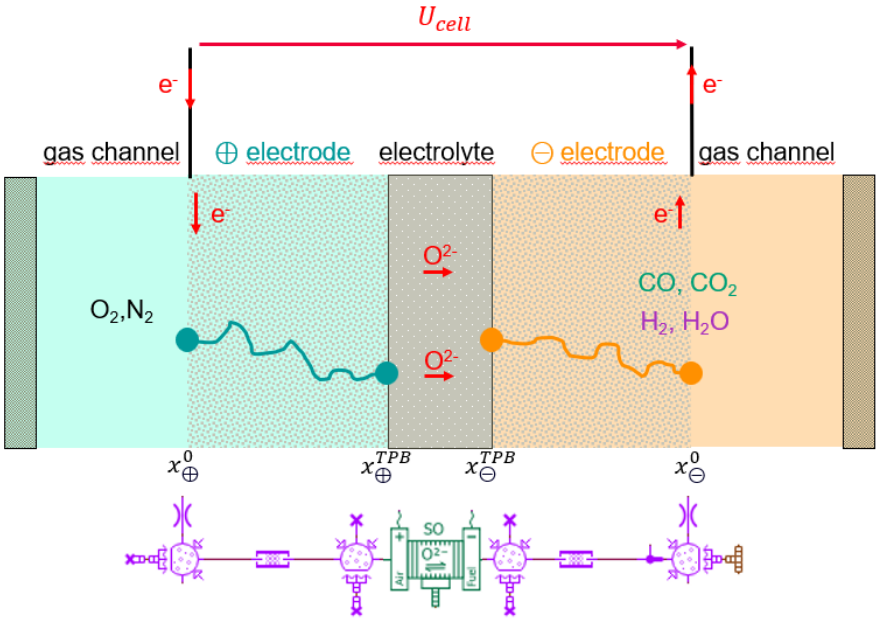

Figure 13: SOFC representation in Amesim

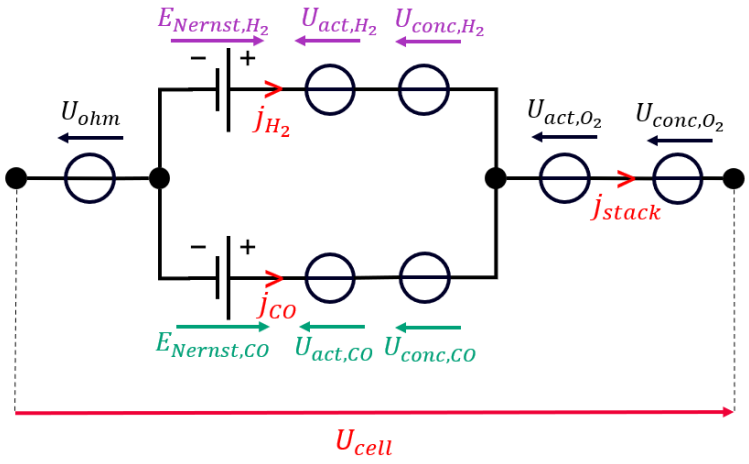

Figure 14: SOFC Equivalent parallel electrical circuit

Solving the electrical circuit, the cell voltage U_{cell} possible to obtain with the SOFC is then given by the ideal (Nernst) overpotential E_{Nernst} for either the CO or the H_2, minus the activation and concentration voltage drops for the same fuel and the total ohmic drop U_{ohm}.

$$U_{cell} = E_{Nernst,H_2} - \overline{U_{act,H_2}} - \overline{U_{conc,H_2}} - \overline{U_{act,O_2}} - \overline{U_{conc,O_2}} - \overline{U_{ohm}} \quad \textit{(Eq. 1)}$$

$$U_{cell} = E_{Nernst,CO} - \overline{U_{act,CO}} - \overline{U_{conc,CO}} - \overline{U_{act,O_2}} - \overline{U_{conc,O_2}} - \overline{U_{ohm}} \quad \textit{(Eq. 2)}$$

The reversible Nernst potential at a reference temperature T_{ref} and pressure P_{ref} can be given to the model as a constant or it can be calculated using the Gibbs Free Energy, the charge transfer number, z, and the Faraday constant F (96485.33 C mol^{-1}).

$$E_{Nernst}(T_{ref}, P_{ref}) = \frac{-\Delta G\ (T_{ref}, P_{ref})}{z\ F} \quad \textit{(Eq. 3)}$$

This value is then adjusted for the cell temperature T:

$$E_{Nernst}(T, P_{ref}) = E_{Nernst}(T_{ref}, P_{ref}) \times \frac{T}{T_{ref}} + \frac{\mathrm{T} - T_{ref}}{T_{ref}} \times \frac{\Delta H_{ref}}{zF} \quad \textit{(Eq. 4)}$$

The cell final reversible potential, considering the temperature T and partial pressures (P_i) dependance, is given by the following equation. As can be seen in Figure 13, the SOFC component receives the partial pressures of the gas in two points, the gas channel, and the triple phase boundary (TPB), which is the contact zone between the electrolyte and electrode. So for the following equations, each of the partial pressures is identifying the point of measure of the pressure, which is either GDL (gas diffusion layer) when is the pressure from the external gas chambers, or TPB, when it's the pressure from the internal gas chambers.

$$E_{Nernst,\,H_2}(P,T) = E_{Nernst,H_2}(T, P_{ref}) + \frac{RT}{zF} \times ln\left(\frac{P^0_{H_2,\,GDL}}{P_{ref}} \times \frac{P_{ref}}{P^0_{H_2O,\,GDL}} \times \left(\frac{P^0_{O_2,\,GDL}}{P_{ref}}\right)^{0.5}\right) \quad \textit{(Eq. 5)}$$

$$E_{Nernst,CO}(P,T) = E_{Nernst,CO}(T, P_{ref}) + \frac{RT}{zF} \times ln\left(\frac{P^0_{CO,\,GDL}}{P_{ref}} \times \frac{P_{ref}}{P^0_{CO_2,\,GDL}} \times \left(\frac{P^0_{O_2,\,GDL}}{P_{ref}}\right)^{0.5}\right) \quad \textit{(Eq. 6)}$$

where R is the universal gas constant (8.3145 J mol^{-1} K^{-1}) and P^0 is the reference pressure, often considered as 1 bar.

There are irreversible electrode reactions which cause a drop on the cell potential. Considering the charge conservation in the circuit analogy, it is possible to obtain the activation overpotentials by solving the Butler-Volmer equations of the current density passing by each branch:

$$j_{stack} = j_{H_2} + j_{CO} \quad \textit{(Eq. 7)}$$

$$j_{H_2} = j^0_{H_2} \times \left[\exp\left(\frac{\alpha_F nF}{RT} \times U_{act,H_2}\right) - \exp\left(\frac{-(1-\alpha_F)nF}{RT} \times U_{act,H_2}\right)\right] \quad \textit{(Eq. 8)}$$

$$j_{CO} = j^0_{CO} \times \left[\exp\left(\frac{\alpha_F nF}{RT} \times U_{act,CO}\right) - \exp\left(\frac{-(1-\alpha_F)nF}{RT} \times U_{act,CO}\right)\right] \quad \textit{(Eq. 9)}$$

$$j_{stack} = j^0_{O_2} \times \left[\exp\left(\frac{\alpha_A nF}{RT} \times U_{act,O_2}\right) - \exp\left(\frac{-(1-\alpha_A)nF}{RT} \times U_{act,O_2}\right)\right] \quad \textit{(Eq. 10)}$$

where j^0 is the exchange current density, α is the charge transfer coefficient and n is the charge transfer number in the rate deterministic step.

The fitting equations for the exchange current density j_i^0 considering the partial pressure relations and temperature are given by:

$$j_{H_2}^0 = \gamma_{H_2} \times \left(\frac{P_{H_2,\,TPB}}{P_{H_2,\,GDL}}\right)^b \left(\frac{P_{H_2O,TPB}}{P_{H_2O,GDL}}\right)^c exp\left(-\frac{E_{act,H_2}}{RT}\right) \quad \textit{(Eq. 11)}$$

$$j_{CO}^0 = \gamma_{CO} \times \left(\frac{P_{CO,TPB}}{P_{CO,GDL}}\right)^b \left(\frac{P_{CO_2,TPB}}{P_{CO_2,GDL}}\right)^c exp\left(-\frac{E_{act,CO}}{RT}\right) \quad \textit{(Eq. 12)}$$

$$j_{O_2}^0 = \gamma_{o_2} \times \left(\frac{P_{O_2,TPB}}{P_{O_2,\,GDL}}\right)^a exp\left(-\frac{E_{act,o_2}}{RT}\right) \quad \textit{(Eq. 13)}$$

Here, γ_i is the pre-exponential factor, $E_{act,i}$ is the activation energy and a,b and c are reaction orders. All those factors need to be fitted to obtain the desired polarization curve.

The concentration losses can be calculated by the semi-empirical model based on the limiting current, shown in (Eq. 14)(Eq. 14, or considering the partial pressures in the GDL and TBP, as shown in (Eq. 15 and (Eq. 16. In the second case, the total concentration loss, U_{conc}, is given by the sum of the losses in the anode and cathode.

$$U_{conc} = -\frac{RT\beta}{zF} \times \ln\left(1 - \frac{j_{stack}}{j_{lim}}\right) \quad \textit{(Eq. 14)}$$

$$U_{conc,\,anode} = \frac{RT}{zF} \times \ln\left(\frac{P_{H_2O,\,TPB}^0}{P_{H_2O,\,GDL}^0} \times \frac{P_{H_2,\,GDL}^0}{P_{H_2,\,TPB}^0}\right) \quad \textit{(Eq. 15)}$$

$$U_{conc,\,\text{cathode}} = \frac{RT}{zF} \times \ln\left(\frac{P_{O_2,\,GDL}^0}{P_{O_2,\,TPB}^0}\right) \quad \textit{(Eq. 16)}$$

$$U_{conc} = U_{conc,\,anode} + U_{conc,\,cathode} \quad \textit{(Eq. 17)}$$

Where the j_{lim} is the limiting current density, which is adjusted together with β for a good fitting of the polarization curve.

Finally, the ohmic overpotential, caused by the resistance of the cell and interconnectors, is given by:

$$U_{ohm} = ASR \times j_{stack} \quad \textit{(Eq. 18)}$$

Where ASR is the area specific resistance of the cell.

For the model validation, all of the parameters of the cell voltage were then fitted with an experimental curve obtained from [48], from a stack operating with methane, under ambient pressure and 700°C. The optimization was done through the Amesim optimizator using NLPQL technique to change the parameters of the system with the goal of minimizing the total sum of the squared errors between model and experimental polarization curve. Each parameter had a upper and lower boundary condition according to literature values to guarantee realistic results, since a large number of combinations of the parameters could reach the same resulting curve. We can see in Figure 15 that the curve behaves as expected and it was possible to obtain a very good fit for our operation range. The obtained parameters are presented in ANEX 1.

It was not possible to obtain experimental data from a stack operating with methane (or oxidizing CO and H2 at the same time) and under various thermodynamic conditions, thus the parameters could only be fitted for a single experimental curve. While this curve gives an estimate for the FC performance, the representativity of the obtained parameters are limited to the conditions of the test. In case of any variation of parameters of temperature, pressure, fuel utilization, fuel composition, etc, the results might diverge from the real operation. For future work, the model should be fitted again with a bigger range of database and more representative I-V curves.

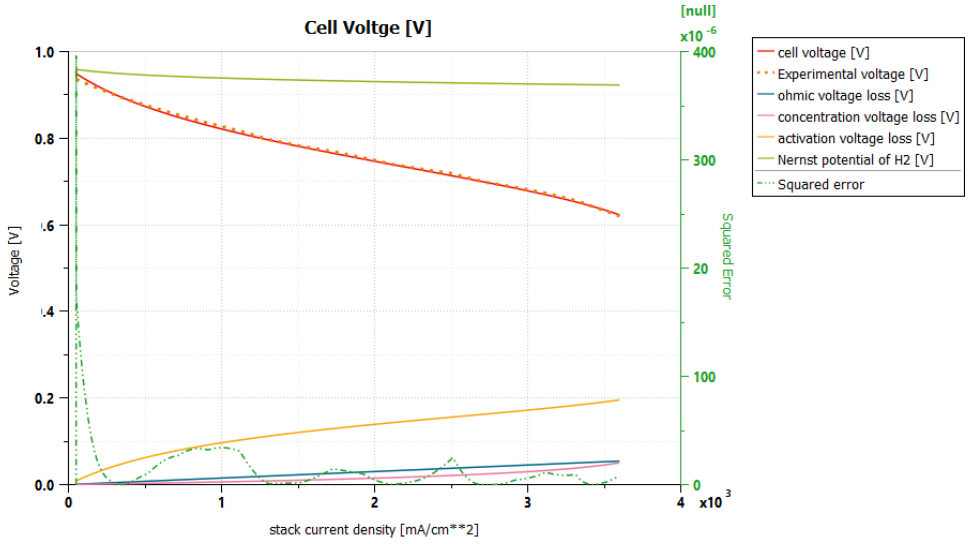

Figure 15: Polarization curve validation

The desired output current is an input, so the molar flux $\dot{n}_i$ of each reactant (H_2, CO and O_2) is given by:

$$\dot{n}_i = -\frac{j_i\, N_{cell}}{z\, F} \qquad \textit{(Eq. 19)}$$

Where N_{cell} is the number of cells in a stack. The molar flux of the products is given by $\dot{n}_{CO_2} = -\dot{n}_{CO}$ and $\dot{n}_{H_2O} = -\dot{n}_{H_2}$.

The stack output electrical power is given by:

$$W_{ele} = U_{cell}\, j_{stack} N_{cell} \qquad \textit{(Eq. 20)}$$

And the heat released by the fuel cell stack, Φ_{stack}, is given by:

$$\Phi_{stack} = \Delta H_{React} - W_{ele} \qquad \textit{(Eq. 21)}$$

Where ΔH_{React} is the enthalpy of the reactions.

The FC electrical efficiency is given by:

$$\eta_{ele} = \frac{U_{cell}}{E_{Nernst,H_2}} \qquad \textit{(Eq. 22)}$$

And lastly, the FC thermodynamic efficiency is given by:

$$\eta_{tn} = \frac{U_{cell}}{E_{Tn,H_2}} \qquad \textit{(Eq. 23)}$$

Where E_{Tn} is the thermoneutral voltage of H_2, given by:

$$E_{Tn} = \frac{-\Delta H}{z\,F} \qquad \textit{(Eq. 24)}$$

4.3.3. Reformer

To operate the fuel cell with fuels other than hydrogen gas, there is the need for a steam reforming reaction, which takes place in the reformer. This reformer can be external, Direct Internal Reformer (DIR) or Indirect Internal Reformer (IIR).

In external reforming, the endothermic steam reforming reaction and the fuel cell reactions are operated separately in the different units, and there is no direct heat transfer between both unit operations. For internal reforming, the endothermic reaction from the steam reforming reaction and the exothermic reaction from the oxidation reaction are operated together in the single unit. For DIR operation, the reforming reaction takes place at the anode of the fuel cell. Heat and steam are supplied directly from the electrochemical reaction, which also helps to complete the reforming reaction by removing and using of hydrogen. For IIR operation, the reforming reaction takes place at the reformer, which is in close thermal contact with the anode side of fuel cell. However, unlike DIR operation, the reformer and anode are operated separately, therefore, the geometry and materials at each section can be different and optimized individually. [49]

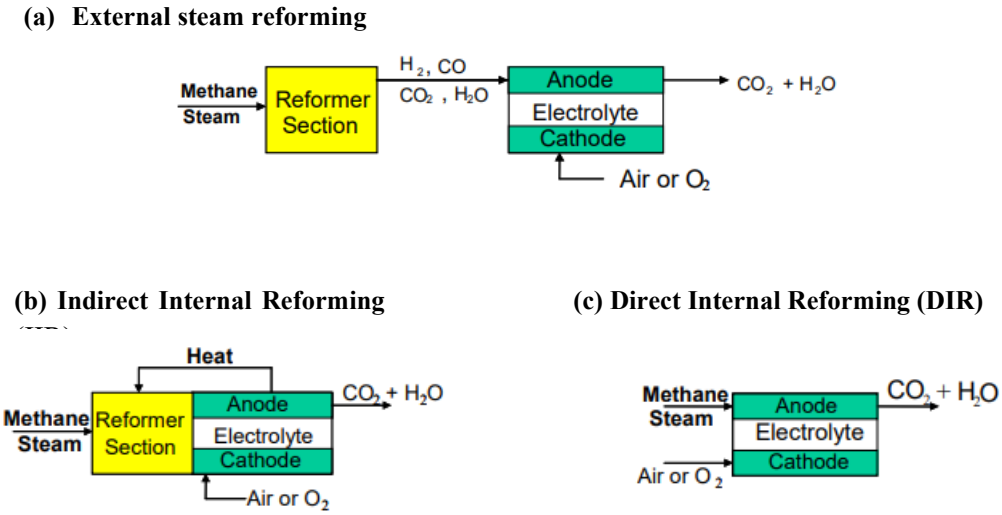

Figure 16: Scheme for methane steam reforming operation for SOFC. Adapted from [49]

With DIR, besides the carbon deposition risk, the kinetics of the reforming reactions are really high at the SOFC operating temperature. This can lead to local subcooling, inhomogeneous temperature distributions and mechanical failure due to thermally induced stress. With the input of excess reforming agent (H_2O, in this case), its possible to completely avoid the formation of carbon deposits, but it also creates a risk of oxidation of the Nickel catalyst in the fuel electrode. [11], [49]

However, there are still many advantages to DIR. Firstly, DIR allows for optimal heat integration in the stack, without any extra heat exchangers and with the endothermic reaction of reforming helping with the cooling of the fuel cell. This reduces drastically the cooling necessities of the stack, allowing to completely avoid the implementation of an external cooling cycle and/or reducing the excess air input in the cathode. Overall, the complexity of the system is reduced, as well as the number/size of some Balance of Plant components, which results in a lower cost for the system installation and operation.[50]

Yang et al. carried out a study to compare internal and external reforming in systems composed of SOFC and gas turbines. He found that, for the same operating parameters, the externally reformed system presented efficiencies between 32% and 60% while the internally reformed system presented between 42% and 70% of efficiency. The reason given for the much lower performance of the externally reformed system is that this system needed a much higher additional fuel to maintain the desired inlet temperature to the Gas Turbine when compared to the alternative system under the same constraints. [19] [51]

For this model, it was chosen to use direct internal reforming. The reformer reactions are accelerated by a nickel catalyst, and the final rate of reactions are dependent on the kinetics, equilibrium and adsorption rates. It was used here as reference the reformer mathematical model developed by Halabi et al. [52], that considers a 4-steps global reactions involving six reactive species (CH_4, O_2, CO, CO_2, H_2, H_2O) and one inert component (N_2) and adiabatic operation. The reactions considered are the methane steam reforming reactions (R4) and (R5), the water gas shift (R8) and the methane full oxidation (R11). For the future it would be interesting to implement a more complex model including the possible formation of carbon depositions.

The combined model for the reaction rate equations can be described as following:

$$R_{R5} = \frac{k_{R5}}{P_{H_2}^{2.5}}\left(P_{CH_4}P_{H_2O} - \frac{P_{H_2}^3 P_{CO}}{K_V}\right) \times \frac{m_{cat}}{\Omega^2} \quad \textit{(Eq. 25)}$$

$$R_{R6} = \frac{k_{R6}}{P_{H_2}^{3.5}}\left(P_{CH_4}P_{H_2O}^2 - \frac{P_{H_2}^4 P_{CO}}{K_{VI}}\right) \times \frac{m_{cat}}{\Omega^2} \quad \textit{(Eq. 26)}$$

$$R_{R7} = \frac{k_{R7}}{P_{H_2}}\left(P_{CO}P_{H_2O} - \frac{P_{H_2}P_{CO_2}}{K_{VII}}\right) \times \frac{m_{cat}}{\Omega^2} \quad \textit{(Eq. 27)}$$

$$R_{R10} = \left(\frac{k_{R10a}P_{CH_4}P_{O_2}}{\left(1 + K_{CH_4}^C P_{CH_4} + K_{O_2}^C P_{O_2}\right)^2} + \frac{k_{R10b}P_{CH_4}P_{O_2}}{1 + K_{CH_4}^C P_{CH_4} + K_{O_2}^C P_{O_2}}\right) m_{cat} \quad \textit{(Eq. 28)}$$

$$\Omega = 1 + \mathrm{K_{CO}}P_{CO} + K_{H_2}P_{H_2} + K_{CH_4}P_{CH_4} + \frac{K_{H_2O}P_{H_2O}}{P_{H_2}} \quad \textit{(Eq. 29)}$$

Where P_i is the partial pressure of each species i, k_{Ri} are the Arrhenius kinetic parameters for each reaction Ri, K_V, K_{VI} and K_{VII} are the equilibrium constants for the respective reactions, K_i^C and K_i are the Van't Hoff parameters for species adsorption. The variable m_{cat} is the mass of catalyst and Ω is the dominator term in the reaction kinetics.

The Arrhenius kinetic rate constant is calculated by:

$$k_{Ri} = A_{Ri} \exp\left(\frac{-E_{a,Ri}}{RT}\right) \quad \textit{(Eq. 30)}$$

The parameters used for the kinetic rate constant and the equilibrium constant equations are presented in Table 3.

Table 3: Reaction equilibrium constants and Arrhenius kinetic parameters

Reaction	Equilibrium Constant	Pre-exponential factor A_{Ri} [mol/kg$_{cat}$/s]	Activation energy $E_{a,Ri}$ [J/mol]
R5	$K_V = \exp\left(\frac{-26830}{T_{catalyst}} + 30.114\right) (bar^2)$	$1.17 \times 10^{15}\ bar^{0.5}$	240 100
R6	$K_{VI} = K_V K_{VII}\ (bar^2)$	$2.83 \times 10^{14}\ bar^{0.5}$	243 900
R7	$K_{VII} = \exp\left(\frac{4400}{T_{catalyst}} - 4.036\right)$	$5.43 \times 10^{5}\ bar^{-1}$	67 130
R10a		$8.11 \times 10^{5}\ bar^{-2}$	86 000
R10b		$6.82 \times 10^{5}\ bar^{-2}$	86 000

The adsorption constants for each species i is calculated by:

$$K_i = A_i \exp\left(\frac{-\Delta H_i}{RT}\right) \quad \textit{(Eq. 31)}$$

$$K_i^C = A_i^C \exp\left(\frac{-\Delta H_i^C}{RT}\right) \quad \textit{(Eq. 32)}$$

The Van't Hoff parameters for species adsorption are presented in Table 4.

Table 4: Van't Hoff parameters for species adsorption

Reaction	A_i [bar^{-1}]	ΔH_i [J/mol]	A_i^C [bar^{-1}]	ΔH_i^C [J/mol]
CH_4	6.65×10^{-4}	-38 280		
CO	8.23×10^{-5}	-70 650		
H_2	6.12×10^{-9}	-82 900		
H_2O	$1.77 \times 10^{5}\ bar$	-88 680		
$CH_4\ (combustion)$			1.26×10^{-1}	-27 300
$O_2\ (combustion)$			7.78×10^{-7}	-92 800

The final enthalpy flow is given by the sum of the enthalpy flows released by each of the reactions and its calculated using the difference in enthalpy from the products and reactants. Each components enthalpy for the instantaneous pressure and temperature is given by a function of the gas mixture library of Amesim.

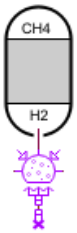

Figure 17: Methane reformer model in Amesim

The performance of the model was validated by the comparison with the data for the equilibrium conversion of methane as a function of temperature, pressure and steam/carbon ratio presented by Joensen et al. [53]. It is possible to see in Figure 18 that the implemented model represents well the methane conversion process for the normal range of operation of a SOFC.

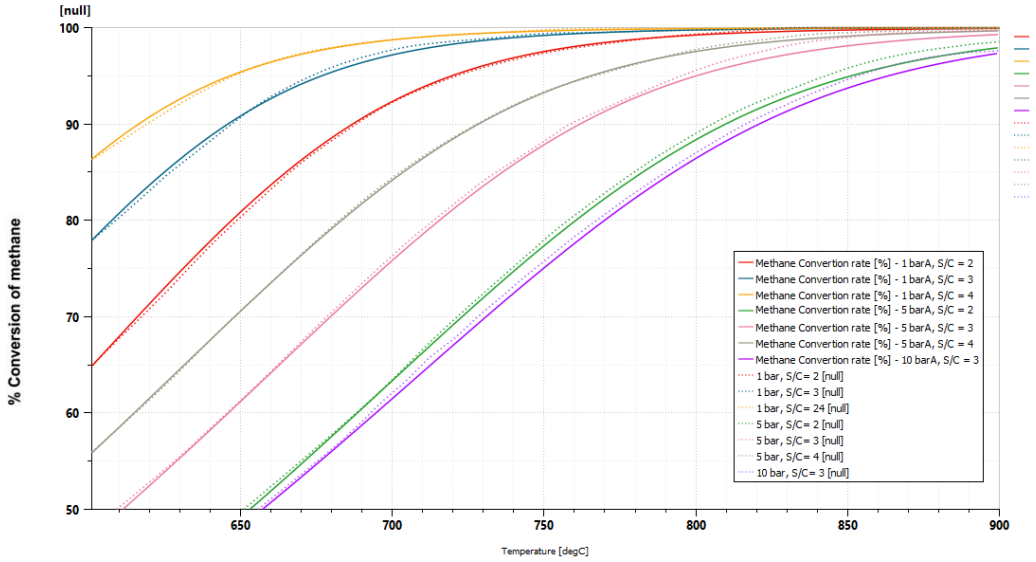

Figure 18: Validation of Methane reformer model.
Equilibrium conversion of methane as a function of temperature, pressure and steam/carbon ratio. In dotted lines are the data by Joensen et al., in full lines are the results from the implemented model in Amesim.

4.3.4. Thermal management

An effective thermal management of the SOFC system is fundamental for the performance of the system. The temperature of the stack affects the entire system's performance, safety and durability. A well designed thermal management can allow the optimal sizing of the system's components, avoiding the overdesign and reducing costs. [54]

During the operation of the fuel cell, the energy released by the reaction, ΔH_{React}, is partially converted into electric power, W_{ele}, while the remaining is converted into heat. This heat, if not removed, will overheat the fuel cell, reducing the system's performance and endangering the components due to thermal stress. Thus, it is important to introduce some cooling, $\Phi_{cooling}$, to maintain the FC at a stable temperature.

When we operate the FC with internal reforming, as explained in the previous section, the endothermic nature of the reaction acts as a partial cooling, decreasing the need of cooling in the system. Besides that, there is also a heat flux from the FC to the environment, $\Phi_{loss,env}$, which depends on the characteristics of the insulation put in place. Overall, to obtain the need of cooling of the SOFC, we can follow the equation:

$$\Phi_{cooling} = \Delta H_{React} - W_{ele} - \Phi_{Reforming} - \Phi_{loss,amb} \qquad \textit{(Eq. 33)}$$

In terms of Amesim model, our electrochemical membrane calculates and outputs through its thermal port the heat remaining in the stack $\Delta H_{React} - W_{ele}$. This heat flux is input into a thermal mass that represents the stack. So, to complete the thermal modeling, we need to output from the stack's thermal mass the heat for the reformer, the heat loss to the environment and whatever is left of energy can be exchanged through forced convection with the cathode and anode mass flows.

In the anode, the fuel is already input at 700°C to improve methane conversion during reforming, and the mass flow is determined by the current density. Considering that, the only inlet flow that we can variate to stabilize the SOFC temperature is the flux of air. Cooling by excess air into the cathode is a very common approach taken for the cooling of SOFC. To achieve this, we can have a temperature sensor in the fuel cell and utilize a PID control to decrease the air inlet if the stack temperature is lower than the desired one and increase the air inlet if the stack temperature is higher than the desired.

When connecting the electrochemical, reformer and thermal models together, we get the scheme for the SOFC stack shown in Figure 19.

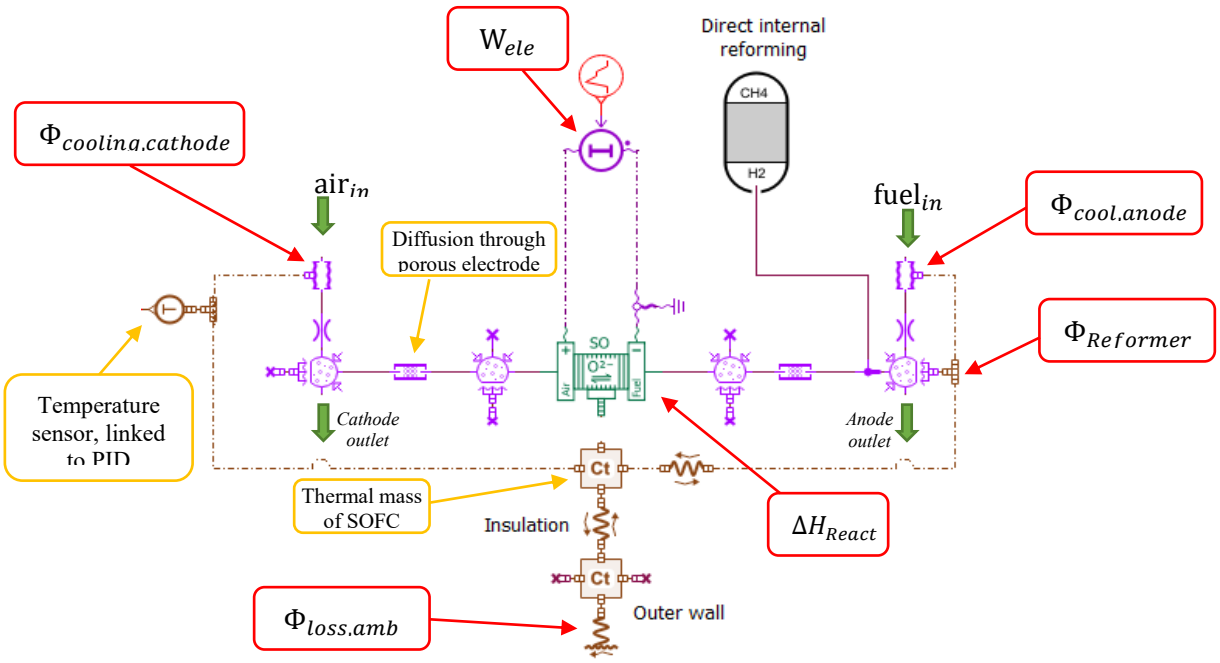

Figure 19: SOFC Amesim model

For this study, the insulation chosen has a thermal conductivity of 0.03W/m/K and thickness of 6cm, based on study results from [55]. The material properties of the FC and outer wall thermal masses are set for LaCrO3 and AISI-316 stainless steel, respectively, and obtained from [56]. The heat loss to the environment is modelled as a convective heat exchange coefficient of 16 W/m²/K, according to study presented in [54] and ambient temperature is considered 20°C. Air is input at 600°C.

The main actor in the cooling of the stack here is in fact the reforming of methane. The choice of fuel utilization ratio (FU) is fundamental, since when we decrease the FU we are absorbing more heat in the reforming process while the FC is not generating more heat, thus leading to higher cooling effect. Furthermore, a decrease in the cell current density (thus increase of operating voltage and electric efficiency) leads to a decrease in heat loss to the stack and consequentially decrease in the excess air needed and size and cost for the ancillary system. This effect is noted in the model developed and confirmed by research from Farhad et al. [26]

The remaining heat balance after reforming and electrochemical reactions to maintain the stack temperature stable is then done by the excess air. For these conditions, we can obtain the air ratio coefficient λ_{air}, which gives the relationship between the minimum necessary air inlet (stoichiometric) and the real input of air.

$$\lambda_{air} = \frac{\dot{n}_{air,real}}{\dot{n}_{air,stoich}} = \frac{\dot{n}_{O_2,real}}{\dot{n}_{O_2,stoich}} \quad \textit{(Eq. 34)}$$

For this calculation, the convective heat exchange coefficient h_{conv} imposed from the fuel cell cathode to the air flow plays a very big role in determining the air excess needed for the cooling. We can see in Figure 20 the change in air ratio coefficient needed to stabilize the system at 700°C, operating at 2A/cm^2 and FU = 80% can fluctuate between 6 and 13 for the h_{conv} of 60 and 25 W/m²/K, respectively. This represents a very big difference in terms of ancillary power consumption of the air blower, so its very important when using the model to choose a relevant heat transfer coefficient. For this study, the model is assuming a value of h_{conv} = 40 W/m²/K.

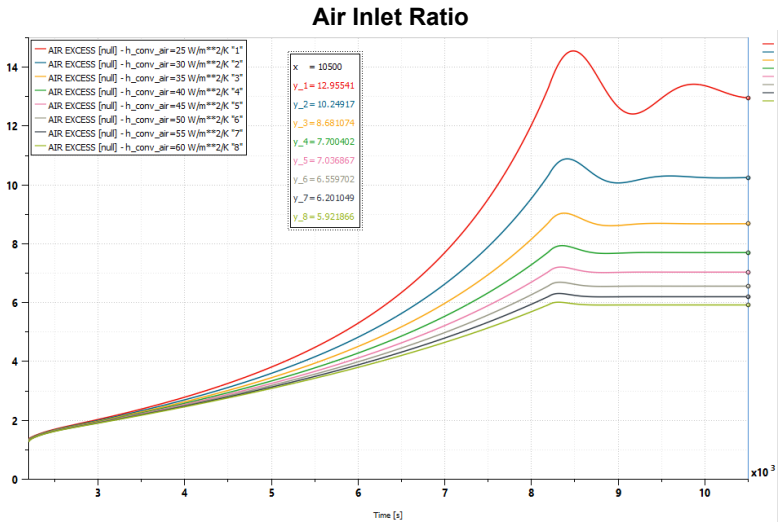

Figure 20: Air ratio for different convective heat exchange coefficients

(the fluctuations in the figure are due to the initial conditions of the dynamic model and settings of the PI control, but do not affect stabilized results)

4.3.5. Anode off gas recirculation (AGR)

The performance of the SOFC is affected by the partial pressure of the components in the stream entering the anode. That's even more true when we consider the internal reforming of the natural gas, since the higher the steam to carbon ratio, the higher is the methane conversion, as shown in Figure 18. To decrease the amount of fresh water that is input to the anode inlet (which requires pre-heating and pumping, thus more energy consumption), we can take advantage of the fact that there is production of water inside the anode and add a recirculation loop. This increases the conversion of unreacted fuels, while decreasing the fresh water input needed for the methane reformation and consequently allowing a size reduction in the ancillary components. [19] [57]

Liso et al. studied a CHP system fueled by natural gas and found an increase of 4.4% in electrical efficiency by adding an anode recycling loop. [57] In the other hand, according to Peters et al., the inclusion of an anode recycle loop in the system can increase the electrical efficiency in up to 16%, but in a system fueled by natural gas with high fuel utilization factor, the efficiency could also decrease due to an increase in ancillary power consumption. [58]

The optimal anode recycling ratio is very dependent on the overall system design: the choice of type, number and size of components, the ancillary power consumption, etc. In the model constructed in this thesis, it was implemented a recirculation loop using a gas pump with variable speed, allowing the

system to vary between 0 and 100% recirculation. With the model complete, this can be used to optimize the ratio for the case in hand.

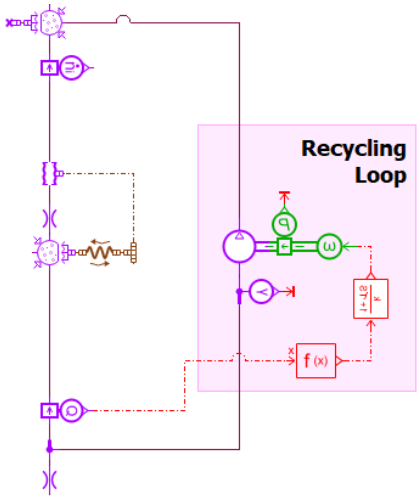

Figure 21: Anode recirculation loop

4.3.6. After Burner

In general, the outlet stream from the fuel cell anode is composed mainly from H_2O and CO_2, but there is also the presence of all the excess fuel: unconverted methane, excess hydrogen and CO. This left over fuels cannot be simply released to the atmosphere, so it is necessary to treat this exhaust gas somehow. In addition, these fuels still have useful energy, which can be converted to heat to increase the overall efficiency of our system. To do that, we implement an afterburner.

An afterburner is simply a combustor used to oxidate the exhaust gas. For this combustion to happen, it is necessary an elevated temperature and the addition of Oxygen to the mixture. In some cases, it is necessary to fire an auxiliary fuel to start the combustion. In principle, if the combustion of the fuels is complete, an environmentally unacceptable vapor is converted completely to CO_2 and H_2O. In practice this is not as simple, since the combustion can be incomplete and generate undesirable partially oxidized species.[59]

Afterburners are usually classified as: Direct-flame, thermal or catalytic afterburner. Both the direct-flame and thermal are operated at a high temperature, generally above 650°C and even higher depending on the fuels in question. The direct-flame method streams the fuel directly through a flame, while the thermal method provides for exposure of the fuels to a high-temperature oxidizing atmosphere for a sufficient time so that the necessary reactions can occur. [59]

The catalytic afterburner can be further classified in low temperature, operating from room temperature up to 500°C, while a hybrid catalytic combustor can operate from 500°C to 1500°C. The catalytic devices incorporate a catalytic surface to accelerate the oxidation reactions and in general require less or no auxiliary fuel. An advantage of this device is that with a good choice of catalyst material, it is possible to avoid unwanted by-products such as nitrogen oxides (NO_x), which are highly pollutant gases. However, catalytic units generally are more expensive and require more maintenance than the other two types of afterburners. [59], [60]

Table 5: Temperatures required to oxidize various compounds

Compound	Ignition Temperature, °C	
	Thermal	Catalytic
Methane	632	500
Carbon Monoxide	609	260
Hydrogen	574	121

From a chemical viewpoint, the detailed mechanisms for the oxidation reactions are very complex and not completely understood. The reactions occur in many complicated sequential and concurrent steps involving a multitude of intermediate species, so it can be quite complicated to model an afterburner based on global reactions, since the reactions' constants change for different stream composition, concentrations and temperature. In general, in the modelling of a combustor, it is used a very extensive and detailed model to fit the parameters for global reactions. [59], [61]

As a general rule, a reaction rate R for a reaction of the type A + B → C, dependent only on thermodynamics and kinetics (without catalyst or equilibrium considerations), is given by:

$$R = k\,[C_A]^{\alpha}\,[C_B]^{\beta} \qquad \textit{(Eq. 35)}$$

Where C means the concentration of the reactant, α and β are the reaction orders, which are determined by experimental fitting, and k is the kinetic rate constant, which is given by:

$$k = A \exp\left(\frac{E_a}{RT}\right) \qquad \textit{(Eq. 36)}$$

Where A and E_a are respectively, the pre-exponential factor and the activation energy for that specific reaction and are usually determined by fitting with experimental data or the results of a detailed reactions mechanism.

For this thesis, to model the afterburner, it was chosen to use a global reactions kinetic mechanism developed by Jones-Lindstedt (JL) [62] and verified by Frassoldati et al. [61] to work well for the combustion of CH_4, H_2 and CO in air. Still according to Frassoldati et al., for the combustion chemistry calculations with excess air, the assumption of a "complete fuel burn" is valid.

The 4-steps reduced global reactions mechanism presented below was then used to simulate numerically the rate of the reactions and components molar flows.

Table 6: Jones-Lindstedt mechanism (JL)

Reaction	Reaction rate
$CH_4 + \frac{1}{2}O_2 \longrightarrow CO + 2H_2$	$r_1 = 4.4 \cdot 10^{11} e^{-\frac{30000}{RT}} [CH_4]^{0.50} [O_2]^{1.25}$
$CH_4 + H_2O \longrightarrow CO + 3H_2$	$r_2 = 3 \cdot 10^{8} e^{-\frac{30000}{RT}} [CH_4][H_2O]$
$CO + H_2O \rightleftarrows CO_2 + H_2$	$r_3 = 2.75 \cdot 10^{9} e^{-\frac{20000}{RT}} [CO][H_2O]$
$H_2 + 0.5O_2 \rightleftarrows H_2O$	$r_4 = 6.80 \cdot 10^{15} T^{-1} e^{-\frac{40000}{RT}} [H_2]^{0.25} [O_2]^{1.50}$

Units of reaction parameters are: cal, mol, l, s.

Typically, in the model, the concentration of the reactants is powered by a factor called the reaction order. When this value is lower than 1, it can cause numerical problems because of possible negative values of the concentration which flag discontinuity issues within the numerical solver. To solve this problem, it was used a linearization technic described by Frassoldati in [61] to correct the reaction rate

expression when the concentration of the reactants become lower than a determined threshold. The final rate constant expression is modified to the following:

$$r = \xi\, k\, C_A^{\alpha} C_B^{\beta} - (1-\xi)\, k\, C_{AT}^{\alpha-1} C_B^{\beta} \qquad \textit{(Eq. 37)}$$

Where k is the kinetic rate constant, C_A is the concentration of the reactant with reaction order lower than 1, α is the reaction order of this reactant, C_{AT} is the defined threshold, and ξ is the function shown below, which is based on hyperbolic tangent and allow the continuous transition. In the following equation, τ and σ are arbitrarily chosen constants.

$$\xi = \frac{1}{2}\left[\tanh\left(\sigma \frac{C_A}{C_{AT}} - \tau\right) + 1\right] \qquad \textit{(Eq. 38)}$$

The described solution adjusts the rate of reaction results as shown in the figure below.

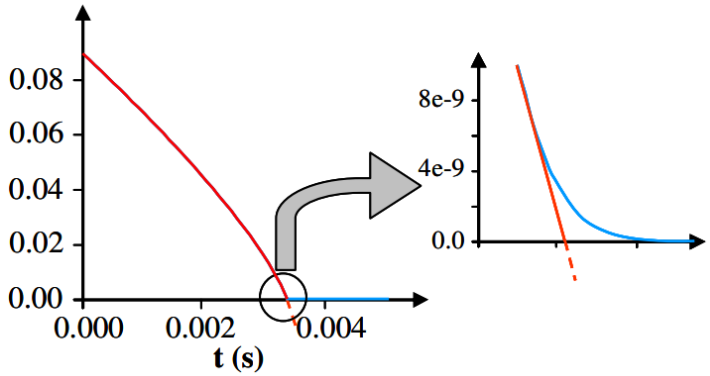

Figure 22: Adjusted rate of reaction with the method described by Frassoldati [61]

The increase in temperature is then given by the enthalpy flow released by each of the reactions and its calculated automatically by the gas mixture library of Amesim.

Finally, after having the model coded into an Amesim component, the performance was evaluated by a results comparison of the same stream inlet conditions in Amesim and a Gibbs reactor implemented in the software ASPEN PLUS. This test was repeated in multiple different conditions with similar results. As an example of results, it was chosen as the inlet for the afterburner the same conditions obtained in the exhaust of an Amesim SOFC model, and for two reference temperatures commonly used in SOFC systems. As can be seen in Table 7, the difference in outputs is very small for most components of the mixture. The higher error of the components H_2, CH_4 and CO is due to the fact that in Aspen there is a nearly complete consumption of the reactants, while the concentration in Amesim is limited by the chosen Threshold as explained above. Overall, all the differences in composition are very small.

The most important factor for our afterburner is that the estimation of the outlet temperature is correct, since that is what will determine the heat possible to recover from the system. As we can see in the table below, the resulting temperature presented a maximum of 0.04% error in comparison with the results from ASPEN PLUS.

Table 7: Comparison of afterburner results between Amesim and Aspen Plus

Component	Inlet	Outlet			
		Aspen	Amesim	Difference	Error %
H_2 [mol/s]	0.001729	9.35E-08	3.19e-11	9.35E-08	99.97
O_2 [mol/s]	0.005133	3.32E-03	3.32E-03	-6.40E-07	-0.0193
H_2O[mol/s]	0.008493	0.010382	0.01038	-1.00E-07	-9.63E-06
CH_4 [mol/s]	8.030E-05	7.35E-30	7.42E-12	-7.42E-12	-
CO [mol/s]	0.001582	5.56E-08	1.42E-06	-1.00E-06	-2449.48
CO_2 [mol/s]	0.000679	0.002342	0.00234	1.36E-06	0.06
N_2 [mol/s]	0.029889	0.029889	0.02989	0	0.00
Temp 1 [°C]	700	1245.56	1245.08	0.48	0.04
Temp 2 [°C]	900	1430.62	1430.19	0.43	0.03

4.3.7. Thermal recovery

In a system including the SOFC, that is working at very high temperatures, it is very important to have a heat recovery system to improve the overall system efficiency without any increase in fuel utilization. The heat recovery here is going to recover the thermal energy from the exhaust gas stream to pre-heat all the inlets and the remaining is going to aid in meeting the heating demands. The most common method to perform this function is the use of heat exchangers, that can be further developed in terms of size and design to optimize the performance. [63]

The model here is considering 4 heat exchangers:

1) Pre-heating of the natural gas from 20°C to 700°C
2) Pre-heating of the water from 20°C to 700°C
3) Pre-heating of the air inlet from 20°C to 600°C
4) The remaining heat available in the exhaust gas is then used to support the heat demand of the house

The geometry of the heat exchangers is not taking into consideration. They are modelled in a very simplified way, where the mass flow is pre-determined by the system's energy requirements, and as inputs we have the inlet temperatures of the hot and cold fluids and one of the desired outlet temperatures. The inlet and outlet temperature for the pre-heating of the fuels is known, so based on that we can obtain the outlet temperature of exhaust gas outlet after each heat exchanger and the amount of heat possible to recover. We can see in Figure 23 the model implemented in Amesim, and in Figure 24 the operating points of the 4 heat exchangers and the heat removed from the exhaust gas.

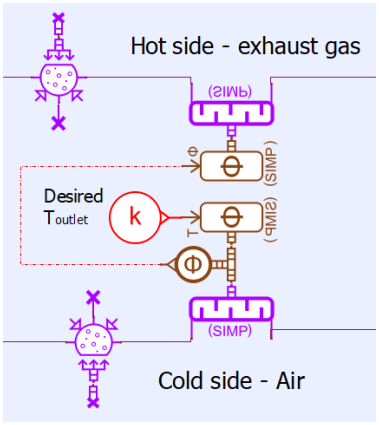

Figure 23: Simplified heat exchanger model in Amesim

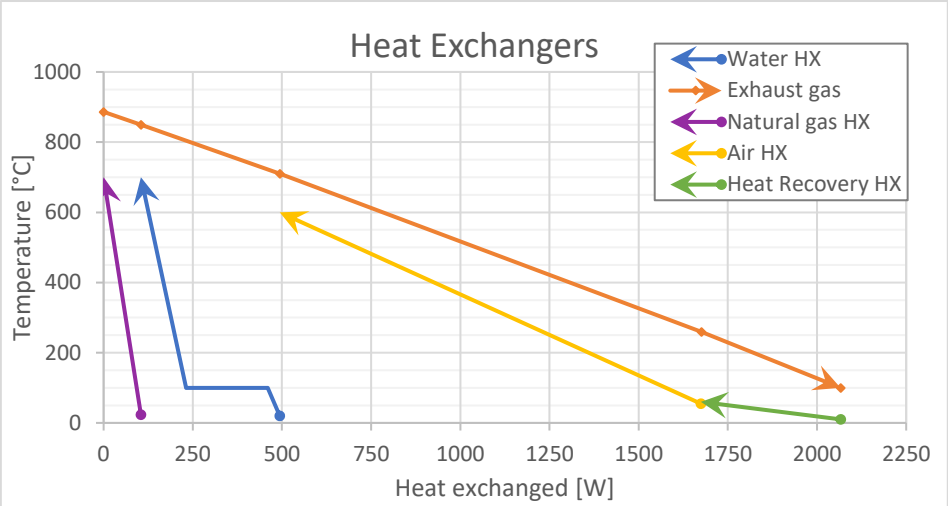

Figure 24: Heat Exchangers operating points

4.3.8. Other ancillaries

According to literature, a natural gas operated SOFC can reach around 335 mbar of pressure drop. [23] For this study, the overall system is considered to have a pressure drop of around 500 mbar in total, which is the value expected to be compensated by the air and fuel blowers.

For simplification of the calculations, all the pumps and blowers are using a conservative total efficiency of 60%, and the AC-DC inverter and DC-DC converters are considering an efficiency of 90%.

5. Results and discussion

The complete model developed is presented in Figure 25. However, as said by Alberto Soto: "*The model in itself is not interesting, but what you can do with it*".

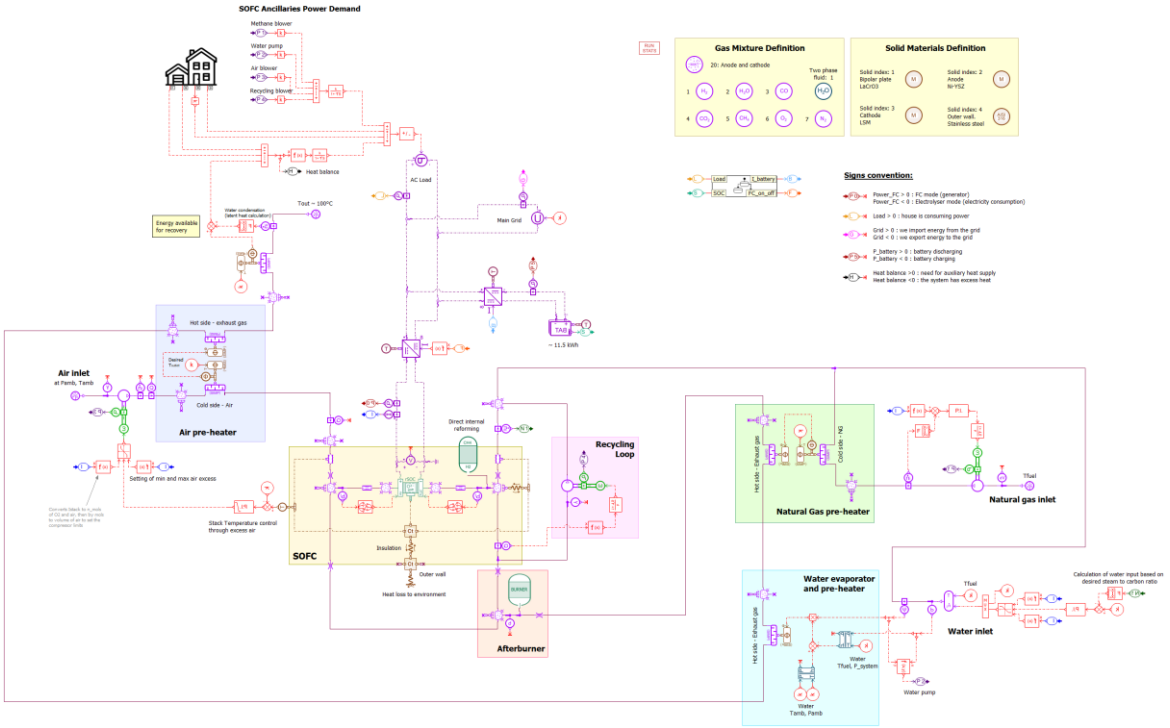

Figure 25: Amesim SOFC-based m-CHP system model developed

From this system we can easily calculate the system efficiencies. For that, we have:

- Cell-stack efficiency: $$\eta_{stack} = \frac{P_{stack}}{\dot{n}_{fuel,in}\, LHV_{fuel}} \quad \textit{(Eq. 39)}$$

- Net system electric efficiency: $$\eta_{AC,net} = \frac{P_{stack}\ \eta_{inverter} - P_{ancillaries}}{\dot{n}_{fuel,in}\, LHV_{fuel}} \quad \textit{(Eq. 40)}$$

- System cogeneration efficiency: $$\eta_{cogen} = \frac{P_{stack}\ \eta_{inverter} - P_{ancillaries} + \dot{Q}_{rec}}{\dot{n}_{fuel,in}\, LHV_{fuel}} \quad \textit{(Eq. 41)}$$

Where P_{stack} is the output DC power produced by the fuel cell stack, $\dot{n}_{fuel,in}$ is the molar flow of fuel input to the system, LHV_{fuel} is the lower heating value of methane, $\eta_{inverter}$ is the efficiency of the DC-AC inverter, $P_{ancillaries}$ is the power consumed by the pump and blowers of the BoP and $\dot{Q}_{rec}$ is the heat recovered from the exhaust gas.

In Table 8 it is presented the results for same system under different current density, fuel utilization and anode recycling inputs, to understand the influence of each of these parameters. The system in itself, in terms of sizing, pressure drops, air inlet temperature, PI control, etc., is not optimised for each of the conditions, so for example when we increase the amount of air that is input into the fuel cell, the pressure of the system also increases, and so on.

Table 8: Comparison of system under different operating conditions

Stack temperature [°C]	700										
Air inlet temperature [°C]	600										
Steam-to-Carbon Ratio	2										
Current Density [mA/cm^2]	500	1000	1500	1000	1000	1000	1000	1000	1000	1000	1000
Fuel utilization CH_4 [%]	80	80	80	60	70	80	90	80	80	80	80
Anode recycling ratio [%]	0	0	0	0	0	0	0	0	0.2	0.4	0.6
Air Ratio	1.7	3.4	5.4	1.0	1.4	3.4	6.9	3.4	3.2	3.15	3.3
Number of Cells	51	26	18	26	26	26	26	26	26	26	26
Power consumed by SOFC ancillaries [W]	5	120	597	7	12	120	692	120	108	100	114
DC Power generated by FC [W]	1145	1145	1145	1145	1145	1145	1145	1145	1145	1145	1145
AC Power generated by FC [W]	1300	1300	1300	1300	1300	1300	1300	1300	1300	1300	1300
Net AC power in system [W]	1295	1180	703	1293	1288	1180	608	1180	1190	1193	1152
Heat possible to recover [W]	752	844	1094	305	1193	844	813	844	840	837	844
LHV of fuel inlet [W]	2133	2220	2280	3021	2515	2220	2048	2220	2212	2202	2188
Stack efficiency [%]	68	65	63	48	57	65	71	65	65	66	66
Net system electric efficiency [%]	61	53	31	43	51	53	30	53	54	54	54
System cogeneration efficiency [%]	96	91	79	53	99	91	69	91	92	93	93

From this, we can start by confirming the influence of the most important operating point parameters in the system's efficiency. When choosing the stack operating current density, there is a compromise to be reached between higher power output and a reasonable stack efficiency. As can be seen in Figure 26, the power of the stack increases as we increase the current density, but so does the fuel that we need to input. This results in a stack efficiency that decreases as the current density increases. Furthermore, a

higher current density implies lower cell voltage, thus more heat released inside the cells and, consequentially, a higher air ratio needed to maintain the temperatures constant.

We can see in Table 8 that to keep the same power output using 500 or 1000 mA/cm^2, the first need nearly double the number of cells, meaning a much higher cost of the stack. However, a lower air ratio means a smaller overall sizing and cost of the auxiliary system, such as compressors and heat exchangers. It would be interesting in the future to analyze and optimize the system taking into consideration the Levelized Cost Of Electricity (LCOE).

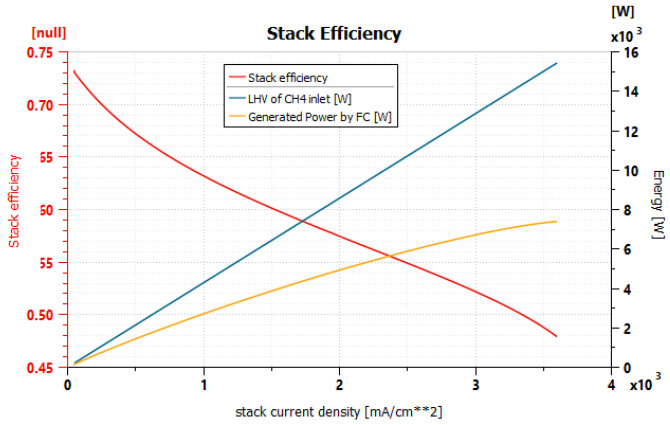

Figure 26: Stack DC efficiency

In the second section of the table, we can see that a system with lower fuel utilization needs a higher fuel input for the same electrical power output, so it has lower stack and electric efficiency, yet the system's efficiency is more tricky. For the 60% FU, too much excess fuel is input into the SOFC, so the electrochemical reactions cannot compensate for the heat removed by the reforming, and it can cause excessive cooling. There, the air inlet is reduced to the minimum possible and the stack still is not capable of maintain its temperature (if the air inlet temperature is maintained at 600°C), so the cell cools down and the efficiency decreases. For the other three cases, the system's efficiency decreases as we increase the fuel utilization. This is because a lower FU implies a lower air ratio and lower parasitic consumption, since there is more fuel, so a higher part of the heat is absorbed by the reforming reaction.

In section three of the table, where we increase the anode recycling ratio, there is an improvement in the conversion of methane in the steam reforming reactions, so we can see, as expected, that the amount of fuel inlet decreases a little. However, there is an increase in the pressure of the system, which increases the parasitic power of blowers, so overall it does not seem, in this particular system, to have a significant improvement by adding anode recirculation.

6. Case Study

To demonstrate some of the potentials of this system, I used it to supply a residential load for a year and then compared the results with some different scenarios which did not utilise the Fuel Cell, allowing to examine the relevancy of the system.

6.1. Energy Demand

The power load was obtained from a dataset published by Schlemminger et al.[64] and it comes from real time measurement of a residential house in Germany. The profile used has a 1-minute temporal resolution and it shows the consumption of the family for the entire year of 2019. The dataset also

contained the ambient temperature (measured every hour) for the location of the house for the same year. A sample of the data used is presented in Figure 27 and Figure 28.

A block was implemented in Amesim to calculate the amount of cooling and heating to maintain the interior of the house always between 20 and 24°C. The house is assumed to be 110 m^2 and to have an overall heat transfer coefficient of 0.432 $W/m^2/°C$. The house hot water consumption assumes the presence of 3 inhabitants and is also calculated by an Amesim block.

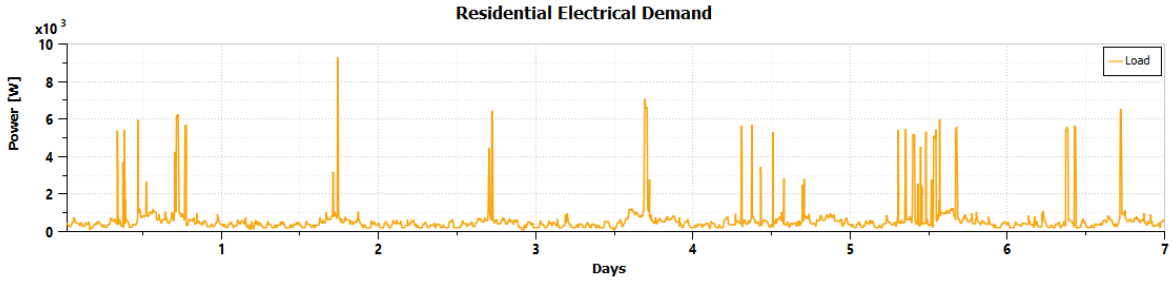

Figure 27: Residential Load profile over a week

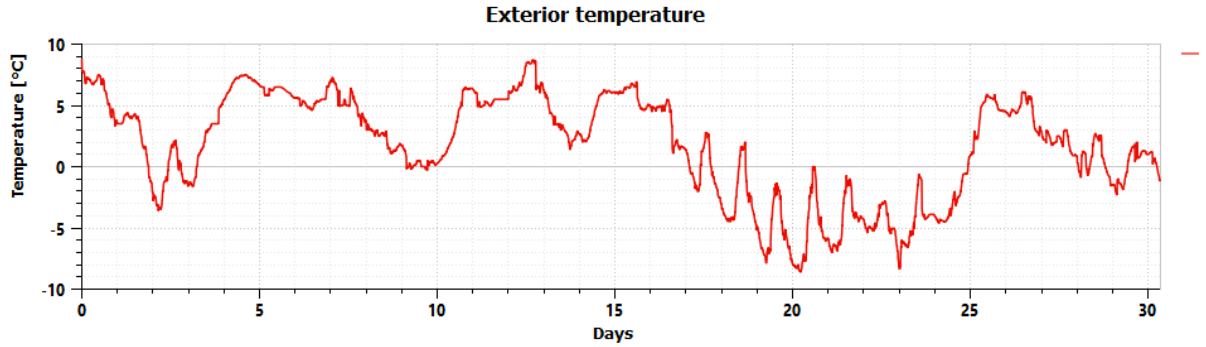

Figure 28:Temperature profile over a month

6.2. Scenarios and assumptions

The system for the case study follows the electrical scheme presented in Figure 29.

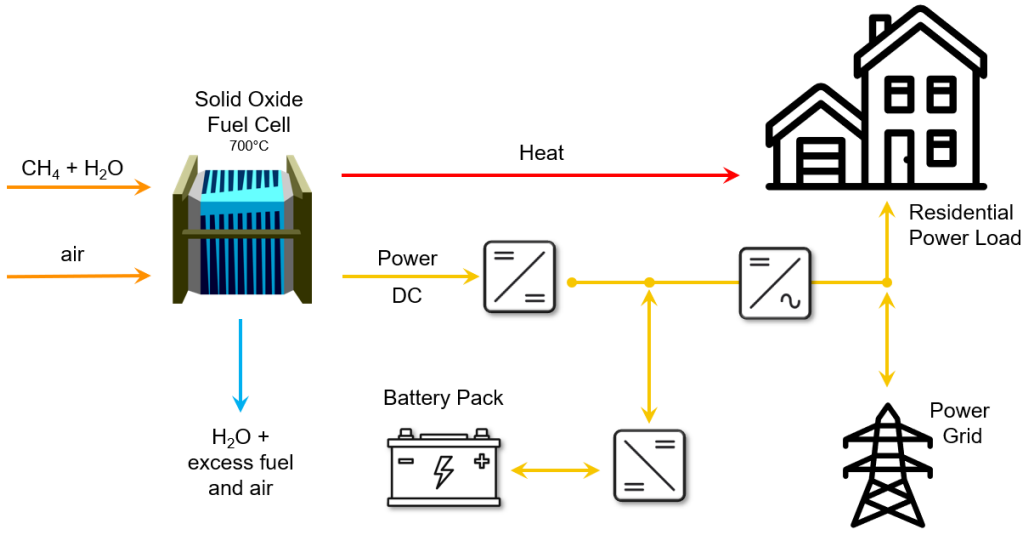

Figure 29: Electrical scheme for case-study

The fuel cell is considered to operate at constant 1.3 kW output power throughout the year. The stack is operating at 1 A/cm^2, 80% fuel utilization and without any anode recirculation, in similar conditions as presented in the previous section. When the electrical load is lower than the power generated by the fuel cell, we use the excess power produced to charge a 11.6 kWh battery pack. Once the battery reaches the maximum State of Charge (SOC) of 95%, we start selling the excess power to the grid. On the other hand, when the load is higher than what is produced, we discharge the battery to help supply the house, and once the battery reaches the minimum SOC of 10%, we buy electricity from the grid.

An example of the power flow working principle is presented in Figure 30.

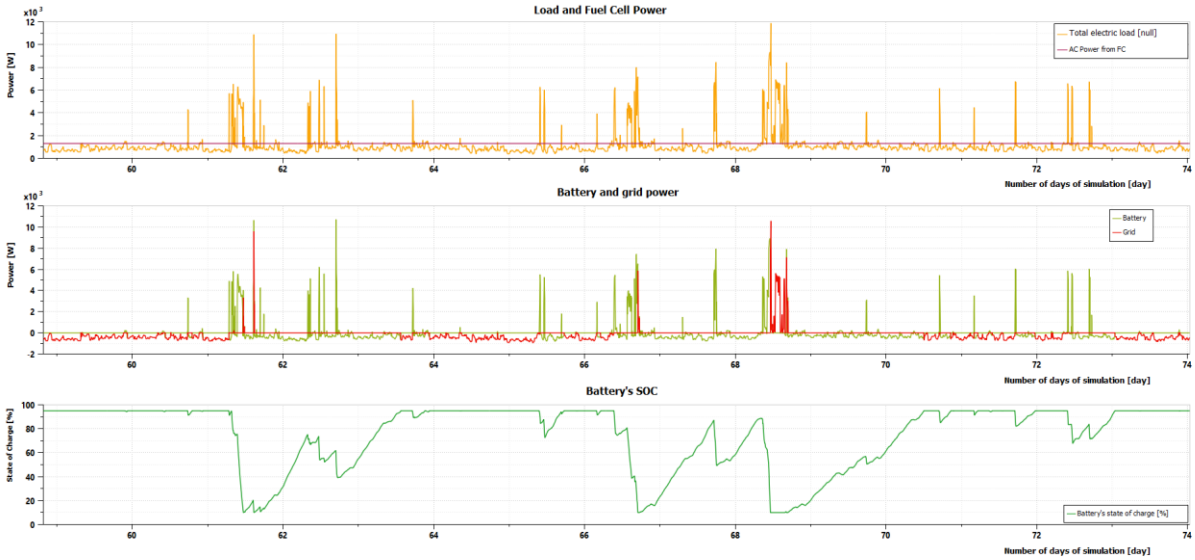

Figure 30: Power flow of the system proposed

For the heat, the heat recovered is deducted from the total heat demand (when there is one) and the remaining heat is assumed to be provided by a heat pump with Coefficient of Performance of heating ($COP_{heating}$) of 3.5. The cooling is also provided by a heat pump with $COP_{cooling}$ of 2.5.

To evaluate this system performance, we will compare it to the energy consumption of a fully electric house, with a house that uses electricity for power and gas for eating needs and a case where the system is supplied by hydrogen instead of natural gas. All of these cases will be applied for both Germany and France since there is a big difference in terms of the electricity and gas prices and carbon emission of its national grids. As a bonus, there is an extra case considering an optimistic view on the price of hydrogen by the year 2030.

As assumptions in energy prices we have:

Table 9: Assumptions on energy prices

Electricity from grid in France (Dec 2022) [65]	0.202	€/kWh
Electricity from grid in Germany (Dec 2022) [66]	0.563	€/kWh
Natural gas in France (Dec 2022) [65]	0.159	€/kWh
Natural gas in Germany (Dec 2022) [66]	0.217	€/kWh
Selling electricity to grid in France (Dec 2021) [67]	0.1	€/kWh
Selling electricity to grid in Germany (2023) [68]	0.086	€/kWh
Hydrogen as fuel in France (2022) [69]	15	€/kg
Hydrogen as fuel in Germany (2023) [70]	13.85	€/kg
Optimistic estimative of Hydrogen price in 2030 [69]	1.5	€/kg

And as assumptions on carbon emissions, we have:

Table 10: Assumptions on carbon emissions

Carbon emissions natural gas [71]	198	g/kWh
Carbon emissions French power sector 2022 [72]	85	g/kWh
Carbon emissions German power sector 2022 [73]	385	g/kWh

6.3. Results

From the system we obtain the following power generation and needs presented in Figure 31. With that, its possible to integrate to have the total energy consumed by the house, produced by the fuel cell, and all the exchanges with the grid. We can see, for example, from the second Grid exchanges shown in red in the figure that the fuel cell is a little over dimensioned for most of the year, so most of the year we have to sell excess energy to the grid. Its also possible to see that the battery is often fully charged, which leads to the conclusion that it might not be a battery pack big enough for the amount of power that needs to be exchanged. The system is not optimised and this simulation for one year took around 4h. This system sizing has potential to be better optimized to reduce exchanges with the grid or increase profitability.

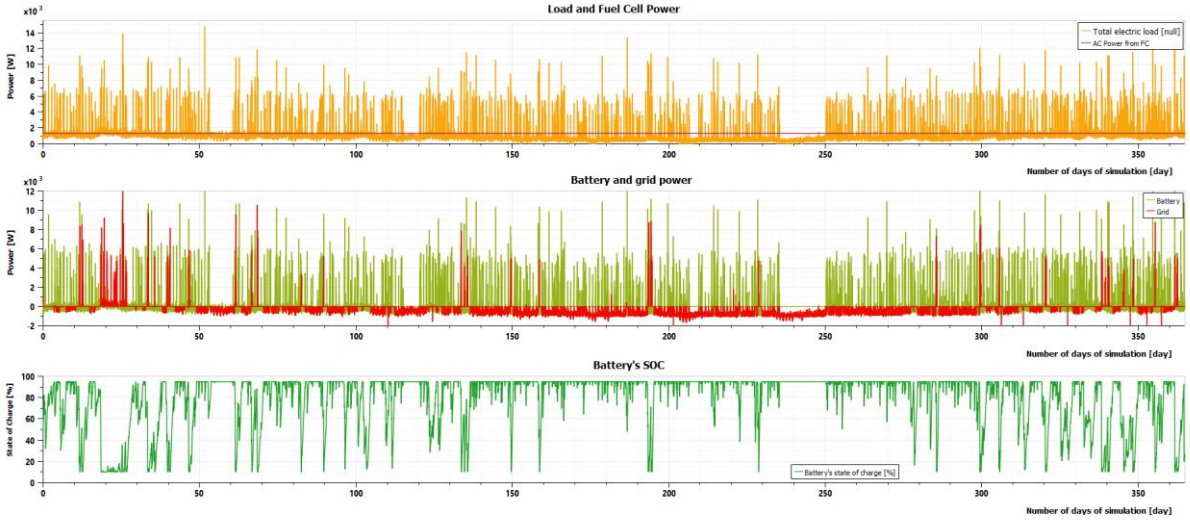

Figure 31: Power flow through the year

From Figure 32 we can compare the total cost, in €, spent to purchase the energy resources for each scenario, and in Figure 33 we can see the equivalent carbon emissions of each as well. We can see that in France, having a fully electric house is the cheapest option, and also the one with the lowest carbon equivalent emissions. This is because of the low and very competitive prices of electricity in France, which has quite a clean energy mix with around 70% of its energy coming from nuclear power. This is different for Germany, where the electricity is more expensive, so the fuel cell can reduce in around 1/3 the cost of energy purchase. In all cases the fuel cell reduces the cost when compared to a house heated by gas.

When we look into the price of the hydrogen scenarios, we can see that for France it costs more than double the price to fuel your FC with hydrogen at current market prices. In Germany the difference is around 1.7 when compared to a FC system using Natural Gas. Hydrogen is not competitive in the market yet. However, with the increase in electrolysis technology and hydrogen production, it is estimated that the price should decrease considerably (some estimations even mention around 10 fold) by 2030. So we

have in pink in the figure the price of the energy if that was the case, which is the cheapest of all the scenarios. While we cannot be as optimistic to invest in that prediction, another more guaranteed option could be to add an electrolyser to the system and produce our own hydrogen. This adds even more complexity to the system but could be an interesting way to decrease operation cost and carbon emissions.

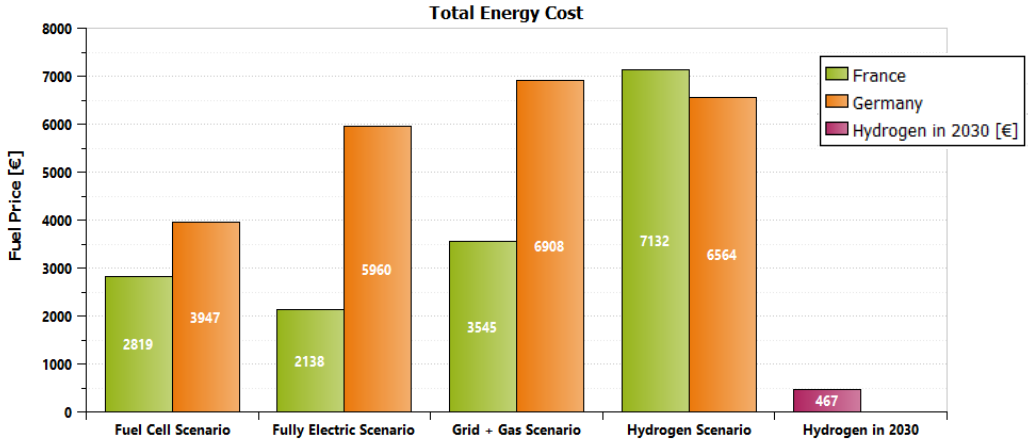

Figure 32: Total cost of fuel for the different scenarios

In Figure 33 we can see that operating the FC using natural gas is not the ideal way to reduce carbon emissions. In fact, in France, it is even contra-productive since the national grid has lower emissions per kWh than the natural gas. In Germany there is a very slight reduction when compared to the fully electric house and a more significant reduction when compared to a house using gas for heating. However, as mentioned before, this system can be a steppingstone to reach the hydrogen scenario in the future once the hydrogen infrastructure is better stablished. Since operating the FC with H_2 has no carbon emissions, when we sell 0 emission energy to the grid, we are in fact lowering the carbon footprint of the grid, so the hydrogen scenario can even reach negative emission values (if the system's production is not well balanced such as is the case here)

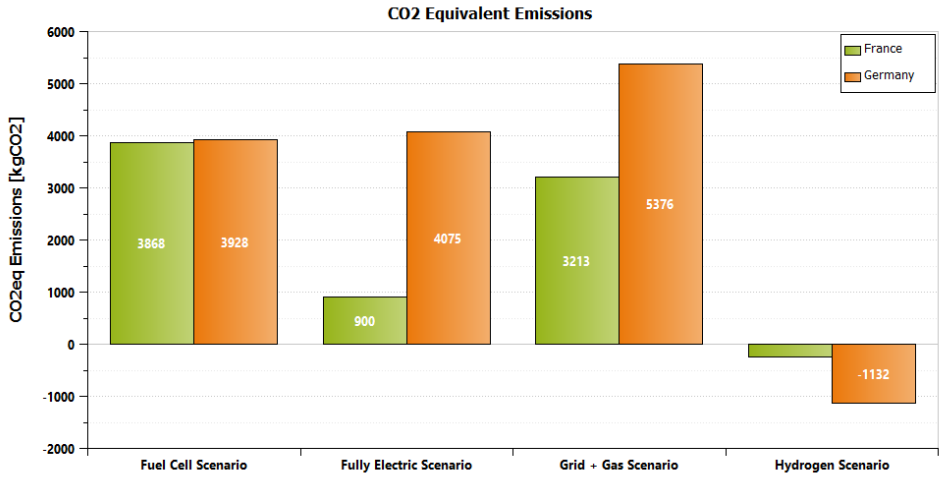

Figure 33: Total carbon equivalent emissions for the different scenarios

7. Conclusions and future work

This model is a first step into a more complex energy system. It allows us to have an insight into the potential of a polygeneration system, to estimate the power flow and cost of energy for a certain system, its carbon emissions, to compare different scenarios, to optimize size and control strategies, etc. However, the simulation time is still very long, considering that the majority of the system is operating at constant output for most of the time. The model needs to be optimized in terms of simulation time to allow a more ease optimization and testing of different operating parameters.

If we maintain the FC operating at a fixed load as it was designed so far, the transient and dynamic response of the BoP is not very relevant and it could be more beneficial to simplify significantly all the FC auxiliary components to improve simulation time. The complex model like it is now can be interesting to simulate the dynamic operation of the FC, for start-up and shut down processes, or more complex control approaches where the FC power output varies with the seasons or even does load following. To do that, more study needs to be done into the time response and limitations of each components of the system and the control approach.

Overall, there is a lot of potential in Amesim for the modelling of microgrids and other complex polygeneration energy systems including Renewable Energy Sources.

If there are future works in this model, some improvements to the model and further increments to the system could be as follows:

- Change of the FC I-V curve and optimization of electrochemical parameters based on multiple polarization curves under different thermodynamic conditions
- Optimization of the operating points of system
- Optimization of the sizing of components such as the fuel cell and battery pack to improve system's performance and efficiency
- Improvement of the simulation time, instabilities and control system
- Study on realistic pressure drops throughout the system
- Try other control and operating strategies, such as operating the cell with power output variation over the year, or even in load following mode
- Optimization of the system's sizing considering the Levelized Cost of Electricity (LCOE)
- Integrate other elements to the system, such as a solar panel and electrolyser
- Operate the SOFC in reversible mode to produce hydrogen when the load is low

8. References

[1] "The Paris Agreement | UNFCCC." https://unfccc.int/process-and-meetings/the-paris-agreement (accessed Jun. 04, 2023).
[2] International Renewable Energy Agency (IRENA), "Energy transition global outlook." https://www.irena.org/Energy-Transition/Outlook (accessed Jun. 04, 2023).
[3] ChooseFrance, "THE FRENCH GREEN HYDROGEN PLAN 2020-2030." [Online]. Available: https://www.tresor.economie.gouv.fr/Articles/4a1ac560-a021-4358-a466-f5430928a1db/files/7d2fd0e2-8a3d-4ce8-bbb3-94cbd5b9c3d1
[4] R. Braun, "Optimal design and operation of solid oxide fuel cell systems for small-scale stationary applications /," 2002.

[5] F.-P. Nagel, "Electricity from wood through the combination of gasification and solid oxide fuel cells: systems analysis and Proof-of-concept," ETH Zurich, 2008. doi: 10.3929/ETHZ-A-005773119.
[6] S. Mukerjee, R. Leah, M. Selby, G. Stevenson, and N. P. Brandon, "Chapter 9 - Life and Reliability of Solid Oxide Fuel Cell-Based Products: A Review," in *Solid Oxide Fuel Cell Lifetime and Reliability*, N. P. Brandon, E. Ruiz-Trejo, and P. Boldrin, Eds., Academic Press, 2017, pp. 173–191. doi: 10.1016/B978-0-08-101102-7.00009-X.
[7] V. Verda and C. Ciano, "Tubular Cells and Stacks," in *Modeling Solid Oxide Fuel Cells: Methods, Procedures and Techniques*, R. Bove and S. Ubertini, Eds., in Fuel Cells and Hydrogen Energy. Dordrecht: Springer Netherlands, 2008, pp. 207–238. doi: 10.1007/978-1-4020-6995-6_7.
[8] S. Hussain and L. Yangping, "Review of solid oxide fuel cell materials: cathode, anode, and electrolyte," *Energy Transitions*, vol. 4, Sep. 2020, doi: 10.1007/s41825-020-00029-8.
[9] L. J. Gauckler *et al.*, "Solid Oxide Fuel Cells: Systems and Materials," no. 12, 2004.
[10] D. P. Minh, T. S. Phan, D. Grouse, and A. Nzihou, "Thermodynamic Equilibrium Study of Methane Reforming with Carbon Dioxide, Water and Oxygen," *JOCET*, vol. 6, no. 4, pp. 309–313, Jul. 2018, doi: 10.18178/JOCET.2018.6.4.480.
[11] L. Fan *et al.*, "Advances on methane reforming in solid oxide fuel cells," *Renewable and Sustainable Energy Reviews*, vol. 166, p. 112646, Sep. 2022, doi: 10.1016/j.rser.2022.112646.
[12] L. Troskialina and R. Steinberger-Wilckens, "The effects of Sn infiltration on dry reforming of biogas at solid oxide fuel cell operating conditions over Ni-YSZ catalysts," *IOP Conference Series: Materials Science and Engineering*, vol. 509, p. 012064, May 2019, doi: 10.1088/1757-899X/509/1/012064.
[13] S. Nai *et al.*, "Review of anodic reactions in hydrocarbon fueled solid oxide fuel cells and strategies to improve anode performance and stability," *Materials for Renewable and Sustainable Energy*, vol. 9, Mar. 2020, doi: 10.1007/s40243-020-0166-8.
[14] "Operation of a solid oxide fuel cell under direct internal reforming of liquid fuels," *Chemical Engineering Journal*, vol. 191, pp. 349–355, May 2012, doi: 10.1016/j.cej.2012.03.030.
[15] "Hydrogen Production: Natural Gas Reforming," *Energy.gov*. https://www.energy.gov/eere/fuelcells/hydrogen-production-natural-gas-reforming (accessed Mar. 24, 2023).
[16] Y. Ru, J. Sang, C. Xia, W.-C. J. Wei, and W. Guan, "Durability of direct internal reforming of methanol as fuel for solid oxide fuel cell with double-sided cathodes," *International Journal of Hydrogen Energy*, vol. 45, no. 11, pp. 7069–7076, Feb. 2020, doi: 10.1016/j.ijhydene.2019.12.222.
[17] Y. Yi, A. D. Rao, J. Brouwer, and G. S. Samuelsen, "Fuel flexibility study of an integrated 25kW SOFC reformer system," *Journal of Power Sources*, vol. 144, no. 1, pp. 67–76, Jun. 2005, doi: 10.1016/j.jpowsour.2004.11.068.
[18] A. Choudhury, H. Chandra, and A. Arora, "Application of solid oxide fuel cell technology for power generation—A review," *Renewable and Sustainable Energy Reviews*, vol. 20, pp. 430–442, Apr. 2013, doi: 10.1016/j.rser.2012.11.031.
[19] O. Corigliano, L. Pagnotta, and P. Fragiacomo, "On the Technology of Solid Oxide Fuel Cell (SOFC) Energy Systems for Stationary Power Generation: A Review," *Sustainability*, vol. 14, no. 22, Art. no. 22, Jan. 2022, doi: 10.3390/su142215276.
[20] S. S. Rathore, S. Biswas, D. Fini, A. P. Kulkarni, and S. Giddey, "Direct ammonia solid-oxide fuel cells: A review of progress and prospects," *International Journal of Hydrogen Energy*, vol. 46, no. 71, pp. 35365–35384, Oct. 2021, doi: 10.1016/j.ijhydene.2021.08.092.
[21] L. Wehrle, Y. Wang, P. Boldrin, N. P. Brandon, O. Deutschmann, and A. Banerjee, "Optimizing Solid Oxide Fuel Cell Performance to Re-evaluate Its Role in the Mobility Sector," *ACS Environ. Au*, vol. 2, no. 1, pp. 42–64, Jan. 2022, doi: 10.1021/acsenvironau.1c00014.
[22] "Processes | Free Full-Text | Solid Oxide Fuel Cell-Based Polygeneration Systems in Residential Applications: A Review of Technology, Energy Planning and Guidelines for Optimizing the Design." https://www.mdpi.com/2227-9717/10/10/2126 (accessed Aug. 08, 2023).
[23] R. J. Braun, S. A. Klein, and D. T. Reindl, "Evaluation of system configurations for solid oxide fuel cell-based micro-combined heat and power generators in residential applications," *Journal of Power Sources*, vol. 158, no. 2, pp. 1290–1305, Aug. 2006, doi: 10.1016/j.jpowsour.2005.10.064.

[24] R. J. Braun, “Techno-Economic Optimal Design of Solid Oxide Fuel Cell Systems for Micro-Combined Heat and Power Applications in the U.S.,” *Journal of Fuel Cell Science and Technology*, vol. 7, no. 031018, Mar. 2010, doi: 10.1115/1.3211099.
[25] L. Tan, X. Dong, C. Chen, Z. Gong, and M. Wang, “Diverse system layouts promising fine performance demonstration: A comprehensive review on present designs of SOFC-based energy systems for building applications,” *Energy Conversion and Management*, vol. 245, p. 114539, Oct. 2021, doi: 10.1016/j.enconman.2021.114539.
[26] S. Farhad, F. Hamdullahpur, and Y. Yoo, “Performance evaluation of different configurations of biogas-fuelled SOFC micro-CHP systems for residential applications,” *International Journal of Hydrogen Energy*, vol. 35, no. 8, pp. 3758–3768, Apr. 2010, doi: 10.1016/j.ijhydene.2010.01.052.
[27] F. Ramadhani, M. A. Hussain, H. Mokhlis, M. Fazly, and J. Mohd. Ali, “Evaluation of solid oxide fuel cell based polygeneration system in residential areas integrating with electric charging and hydrogen fueling stations for vehicles,” *Applied Energy*, vol. 238, pp. 1373–1388, Mar. 2019, doi: 10.1016/j.apenergy.2019.01.150.
[28] T. Elmer, M. Worall, S. Wu, and S. Riffat, “Assessment of a novel solid oxide fuel cell tri-generation system for building applications,” *Energy Conversion and Management*, vol. 124, pp. 29–41, Sep. 2016, doi: 10.1016/j.enconman.2016.07.010.
[29] V. Cigolotti, M. Genovese, and P. Fragiacomo, “Comprehensive Review on Fuel Cell Technology for Stationary Applications as Sustainable and Efficient Poly-Generation Energy Systems,” *Energies*, vol. 14, no. 16, Art. no. 16, Jan. 2021, doi: 10.3390/en14164963.
[30] R. J. Braun and P. Kazempoor, “CHAPTER 12. Application of SOFCs in Combined Heat, Cooling and Power Systems,” in *Energy and Environment Series*, M. Ni and T. S. Zhao, Eds., Cambridge: Royal Society of Chemistry, 2013, pp. 327–382. doi: 10.1039/9781849737777-00327.
[31] P. Marocco, M. Gandiglio, and M. Santarelli, “When SOFC-based cogeneration systems become convenient? A cost-optimal analysis,” *Energy Reports*, vol. 8, pp. 8709–8721, Nov. 2022, doi: 10.1016/j.egyr.2022.06.015.
[32] R. K. Akikur, R. Saidur, K. R. Ullah, S. A. Hajimolana, H. W. Ping, and M. A. Hussain, “Economic feasibility analysis of a solar energy and solid oxide fuel cell-based cogeneration system in Malaysia,” *Clean Techn Environ Policy*, vol. 18, no. 3, pp. 669–687, Mar. 2016, doi: 10.1007/s10098-015-1050-6.
[33] “HEATSTACK – project achievements and results » HEATSTACK Project,” *HEATSTACK Project*, Mar. 23, 2020. http://www.heatstack.eu/news-and-events/heatstack-project-achievements-results/ (accessed Aug. 08, 2023).
[34] “大阪ガス：世界最高効率を更新した家庭用燃料電池「エネファームtype Ｓ」の新製品発売及び「エネファーム」の累計販売台数8万台突破について.” https://www.osakagas.co.jp/company/press/pr_2018/1268655_37838.html (accessed Aug. 08, 2023).
[35] Erik Schumacher, “Callux, fuel cell for domestic households – practical test,” Oct. 2015. [Online]. Available: http://enefield.eu/wp-content/uploads/2015/09/NIP-Vollversammlung_Callux_engl_15-05-05.pdf
[36] “ene.field » About.” https://enefield.eu/category/about/ (accessed Aug. 08, 2023).
[37] E. R. Nielsen *et al.*, “Status on Demonstration of Fuel Cell Based Micro-CHP Units in Europe,” *Fuel Cells*, vol. 19, no. 4, pp. 340–345, 2019, doi: 10.1002/fuce.201800189.
[38] M.-H. Chen and T. L. Jiang, “The analyses of the heat-up process of a planar, anode-supported solid oxide fuel cell using the dual-channel heating strategy,” *International Journal of Hydrogen Energy*, vol. 36, no. 11, pp. 6882–6893, Jun. 2011, doi: 10.1016/j.ijhydene.2011.02.129.
[39] M. Halinen, O. Thomann, and J. Kiviaho, “Experimental study of SOFC system heat-up without safety gases,” *International Journal of Hydrogen Energy*, vol. 39, no. 1, pp. 552–561, Jan. 2014, doi: 10.1016/j.ijhydene.2013.10.043.
[40] K. W. Eichhorn Colombo and V. V. Kharton, “Start-Up of a Solid Oxide Fuel Cell System with a View to Materials Science-Related Aspects, Control and Thermo-Mechanical Stresses,” *Crystals*, vol. 11, no. 7, Art. no. 7, Jul. 2021, doi: 10.3390/cryst11070732.
[41] M.-H. Chen and T. L. Jiang, “The analyses of the start-up process of a planar, anode-supported solid oxide fuel cell using three different start-up procedures,” *Journal of Power Sources*, vol. 220, pp. 331–341, Dec. 2012, doi: 10.1016/j.jpowsour.2012.08.018.

[42] A. M. Beney, “Investigation into the Heat Up Time for Solid Oxide Fuel Cells in Automotive Applications,” University of Guelph.
[43] R. Napoli, M. Gandiglio, A. Lanzini, and M. Santarelli, “Techno-economic analysis of PEMFC and SOFC micro-CHP fuel cell systems for the residential sector,” *Energy and Buildings*, vol. 103, pp. 131–146, Sep. 2015, doi: 10.1016/j.enbuild.2015.06.052.
[44] B. Zhang *et al.*, “Rapid load transition for integrated solid oxide fuel cell – Gas turbine (SOFC-GT) energy systems: A demonstration of the potential for grid response,” *Energy Conversion and Management*, vol. 258, p. 115544, Apr. 2022, doi: 10.1016/j.enconman.2022.115544.
[45] “On reprend les bases : quelle est la composition du gaz naturel ?,” *Le maGAZine*, Jun. 05, 2019. https://www.sefe-energy.fr/gazmagazine/2019/06/composition-gaz-naturel/ (accessed Jun. 15, 2023).
[46] L. Andreassi, C. Toro, and S. Ubertini, “Modeling Carbon Monoxide Direct Oxidation in Solid Oxide Fuel Cells,” *Journal of Fuel Cell Science and Technology*, vol. 6, no. 2, p. 021307, May 2009, doi: 10.1115/1.3080552.
[47] Z. Lyu *et al.*, “Comparison of off-gas utilization modes for solid oxide fuel cell stacks based on a semi-empirical parametric model,” *Applied Energy*, vol. 270, p. 115220, Jul. 2020, doi: 10.1016/j.apenergy.2020.115220.
[48] Nguyen Q. Minh, “Innovative, Versatile, and Cost-Effective Solid Oxide Fuel Cell Stack Concept,” University of California San Diego, Center for Energy Research, Jul. 2020. [Online]. Available: https://netl.doe.gov/sites/default/files/netl-file/20SOFC_Minh.pdf
[49] N. Laosiripojana, W. Wiyaratn, W. Kiatkittipong, A. Arpornwichanop, A. Soottitantawat, and S. Assabumrungrat, “Reviews on Solid Oxide Fuel Cell Technology,” *Engineering Journal*, vol. 13, no. 1, pp. 65–84, Feb. 2009, doi: 10.4186/ej.2009.13.1.65.
[50] L. van Biert, M. Godjevac, K. Visser, and P. V. Aravind, “Dynamic modelling of a direct internal reforming solid oxide fuel cell stack based on single cell experiments,” *Applied Energy*, vol. 250, pp. 976–990, Sep. 2019, doi: 10.1016/j.apenergy.2019.05.053.
[51] W. J. Yang, S. K. Park, T. S. Kim, J. H. Kim, J. L. Sohn, and S. T. Ro, “Design performance analysis of pressurized solid oxide fuel cell/gas turbine hybrid systems considering temperature constraints,” *Journal of Power Sources*, vol. 160, no. 1, pp. 462–473, Sep. 2006, doi: 10.1016/j.jpowsour.2006.01.018.
[52] M. H. Halabi, M. H. J. M. de Croon, J. van der Schaaf, P. D. Cobden, and J. C. Schouten, “Modeling and analysis of autothermal reforming of methane to hydrogen in a fixed bed reformer,” *Chemical Engineering Journal*, vol. 137, no. 3, pp. 568–578, Apr. 2008, doi: 10.1016/j.cej.2007.05.019.
[53] F. Joensen and J. R. Rostrup-Nielsen, “Conversion of hydrocarbons and alcohols for fuel cells,” *Journal of Power Sources*, vol. 105, no. 2, pp. 195–201, Mar. 2002, doi: 10.1016/S0378-7753(01)00939-9.
[54] K. Kattke and R. Braun, “Implementing Thermal Management Modeling Into SOFC System-Level Design,” *Journal of Fuel Cell Science and Technology*, vol. 8, pp. 1–12, Apr. 2011, doi: 10.1115/1.4002233.
[55] T. Shimada, T. Kato, and Y. Tanaka, “Numerical Analysis of Thermal Behavior of Small Solid Oxide Fuel Cell Systems,” *Journal of Fuel Cell Science and Technology - J FUEL CELL SCI TECHNOL*, vol. 4, Aug. 2007, doi: 10.1115/1.2744049.
[56] P. Pianko-Oprych, T. Zinko, and Z. Jaworski, “A Numerical Investigation of the Thermal Stresses of a Planar Solid Oxide Fuel Cell,” *Materials (Basel)*, vol. 9, no. 10, p. 814, Sep. 2016, doi: 10.3390/ma9100814.
[57] V. Liso, A. C. Olesen, M. P. Nielsen, and S. K. Kær, “Performance comparison between partial oxidation and methane steam reforming processes for solid oxide fuel cell (SOFC) micro combined heat and power (CHP) system,” *Energy*, vol. 36, no. 7, pp. 4216–4226, Jul. 2011, doi: 10.1016/j.energy.2011.04.022.
[58] R. Peters, R. Deja, L. Blum, J. Pennanen, J. Kiviaho, and T. Hakala, “Analysis of solid oxide fuel cell system concepts with anode recycling,” *International Journal of Hydrogen Energy*, vol. 38, no. 16, pp. 6809–6820, May 2013, doi: 10.1016/j.ijhydene.2013.03.110.
[59] US Environmental Protection Agency, “Chemical Aspects of Afterburner Systems.” https://nepis.epa.gov/Exe/ZyNET.exe/9101K6W9.TXT?ZyActionD=ZyDocument&Client=EPA&Index=1976+Thru+1980&Docs=&Query=&Time=&EndTime=&SearchMethod=1&TocRestric

t=n&Toc=&TocEntry=&QField=&QFieldYear=&QFieldMonth=&QFieldDay=&IntQFieldOp=0&ExtQFieldOp=0&XmlQuery=&File=D%3A%5Czyfiles%5CIndex%20Data%5C76thru80%5CTxt%5C00000031%5C9101K6W9.txt&User=ANONYMOUS&Password=anonymous&SortMethod=h%7C-&MaximumDocuments=1&FuzzyDegree=0&ImageQuality=r75g8/r75g8/x150y150g16/i425&Display=hpfr&DefSeekPage=x&SearchBack=ZyActionL&Back=ZyActionS&BackDesc=Results%20page&MaximumPages=1&ZyEntry=1&SeekPage=x&ZyPURL (accessed Jun. 09, 2023).

[60] J. Kim, J. Yu, S. Lee, A. Tahmasebi, C.-H. Jeon, and J. Lucas, "Advances in catalytic hydrogen combustion research: Catalysts, mechanism, kinetics, and reactor designs," *International Journal of Hydrogen Energy*, vol. 46, no. 80, pp. 40073–40104, Nov. 2021, doi: 10.1016/j.ijhydene.2021.09.236.

[61] A. Frassoldati, A. Cuoci, T. Faravelli, E. Ranzi, C. Candusso, and D. Tolazzi, "Simplified kinetic schemes for oxy-fuel combustion," 2009.

[62] W. P. Jones and R. P. Lindstedt, "Global reaction schemes for hydrocarbon combustion," *Combustion and Flame*, vol. 73, no. 3, pp. 233–249, Sep. 1988, doi: 10.1016/0010-2180(88)90021-1.

[63] F. Ramadhani, M. A. Hussain, H. Mokhlis, and O. Erixno, "Solid Oxide Fuel Cell-Based Polygeneration Systems in Residential Applications: A Review of Technology, Energy Planning and Guidelines for Optimizing the Design," *Processes*, vol. 10, no. 10, Art. no. 10, Oct. 2022, doi: 10.3390/pr10102126.

[64] M. Schlemminger, T. Ohrdes, E. Schneider, and M. Knoop, "Dataset on electrical single-family house and heat pump load profiles in Germany," *Sci Data*, vol. 9, no. 1, Art. no. 1, Feb. 2022, doi: 10.1038/s41597-022-01156-1.

[65] "France energy prices," *GlobalPetrolPrices.com*. https://www.globalpetrolprices.com/France/ (accessed Sep. 06, 2023).

[66] "Germany energy prices," *GlobalPetrolPrices.com*. https://www.globalpetrolprices.com/Germany/ (accessed Sep. 06, 2023).

[67] "Tout savoir sur l'obligation d'achat solaire (OA) du photovoltaïque," Aug. 23, 2022. https://mypower.engie.fr/conseils/aides-panneaux-solaires/oa-solaire.html (accessed Sep. 06, 2023).

[68] "Germany raises feed-in tariffs for solar up to 750 kW," *pv magazine International*, Jul. 07, 2022. https://www.pv-magazine.com/2022/07/07/germany-raises-feed-in-tariffs-for-solar-up-to-750-kw/ (accessed Sep. 06, 2023).

[69] "Hydrogen fuel price in France. Updated." https://www.glpautogas.info/en/hydrogen-sale-price-france.html (accessed Sep. 06, 2023).

[70] "Hydrogen fuel price Worldwide. Updated." https://www.glpautogas.info/en/hydrogen-sale-price.html (accessed Sep. 06, 2023).

[71] "How much CO2 does my home emit?," *Energuide*. https://www.energuide.be/en/questions-answers/how-much-co2-does-my-home-emit/68/ (accessed Sep. 06, 2023).

[72] "France: power sector carbon intensity 2022," *Statista*. https://www.statista.com/statistics/1290216/carbon-intensity-power-sector-france/ (accessed Sep. 06, 2023).

[73] "Germany: power sector carbon intensity 2022," *Statista*. https://www.statista.com/statistics/1290224/carbon-intensity-power-sector-germany/ (accessed Sep. 06, 2023).

9. ANEX 1 – Fitting parameters for Fuel Cell

Name	Title	Value	Unit
▾ Activation losses			
alpha_cathode	charge transfer coefficient at air electrode	**0.69493**	null
alpha_anode	charge transfer coefficient at fuel electrode	**0.49989**	null
Ya_O2	pre exponential factor for O2 at air electrode	**33217300000**	mA/cm**2
Yf_H2	pre exponential factor for H2 at fuel electrode	**3229250000**	mA/cm**2
Yf_CO	pre exponential factor for CO at fuel electrode	**32292500**	mA/cm**2
Eacta_O2	Activation energy for O2 at air electrode	**151.6837**	kJ/mol
Eactf_H2	Activation energy for H2 at fuel electrode	**99.18504**	kJ/mol
Eactf_CO	Activation energy for CO at fuel electrode	**99.18504**	kJ/mol
a_O2	c exponent for O2 exchange current density	**0**	null
b_H2	a exponent for H2 exchange current density	**0**	null
c_H2	b exponent for H2 exchange current density	**0**	null
b_CO	a exponent for CO exchange current density	**0**	null
c_CO	b exponent for CO exchange current density	**0**	null
▾ Concentration and ohmic losses			
ASR	Area specific resistance	0.01505	Ohm*cm**2
conc_fitting	Fitting parameter for concentration voltage loss	2.0059	null
j_limit_pos	Limiting current density for concentration voltage loss	3962.16894	mA/cm**2